



Cite this: *Mol. Syst. Des. Eng.*, 2022, **7**, 1707

# Computational investigation of multifunctional MOFs for adsorption and membrane-based separation of CF<sub>4</sub>/CH<sub>4</sub>, CH<sub>4</sub>/H<sub>2</sub>, CH<sub>4</sub>/N<sub>2</sub>, and N<sub>2</sub>/H<sub>2</sub> mixtures†

Hakan Demir \* and Seda Keskin \*

The ease of functionalization of metal–organic frameworks (MOFs) can unlock unprecedented opportunities for gas adsorption and separation applications as the functional groups can impart favorable/unfavorable regions/interactions for the desired/undesired adsorbates. In this study, the effects of the presence of multiple functional groups in MOFs on their CF<sub>4</sub>/CH<sub>4</sub>, CH<sub>4</sub>/H<sub>2</sub>, CH<sub>4</sub>/N<sub>2</sub>, and N<sub>2</sub>/H<sub>2</sub> separation performances were computationally investigated combining grand canonical Monte Carlo (GCMC) and molecular dynamics (MD) simulations. The most promising adsorbents showing the best combinations of selectivity, working capacity, and regenerability were identified for each gas separation. 15, 13, and 16 out of the top 20 MOFs identified for the CH<sub>4</sub>/H<sub>2</sub>, CH<sub>4</sub>/N<sub>2</sub>, and N<sub>2</sub>/H<sub>2</sub> adsorption-based separation, respectively, were found to have –OCH<sub>3</sub> groups as one of the functional groups. The biggest improvements in CF<sub>4</sub>/CH<sub>4</sub>, CH<sub>4</sub>/H<sub>2</sub>, CH<sub>4</sub>/N<sub>2</sub>, and N<sub>2</sub>/H<sub>2</sub> selectivities were found to be induced by the presence of –OCH<sub>3</sub>–OCH<sub>3</sub> groups in MOFs. For CH<sub>4</sub>/H<sub>2</sub> separation, MOFs with two and three functionalized linkers were the best adsorbent candidates while for N<sub>2</sub>/H<sub>2</sub> separation, all the top 20 materials involve two functional groups. Membrane performances of the MOFs were also studied for CH<sub>4</sub>/H<sub>2</sub> and CH<sub>4</sub>/N<sub>2</sub> separation and the results showed that MOFs having –F–NH<sub>2</sub> and –F–OCH<sub>3</sub> functional groups present the highest separation performances considering both the membrane selectivity and permeability.

Received 1st July 2022,  
Accepted 25th August 2022

DOI: 10.1039/d2me00130f

[rsc.li/molecular-engineering](https://rsc.li/molecular-engineering)

## Design, System, Application

Metal–organic frameworks (MOFs) have appeared as promising candidates for various gas separations as they possess wider structural and chemical diversity than conventional materials such as activated carbon and zeolites. Thus far, many studies focused on the construction and/or testing of MOFs with single linker for gas separation applications. Multivariate MOFs (MTV-MOFs), which have multiple linker types, can supersede the gas separation performances of single-linker MOFs through synergistic effects of multiple linker types and/or functional groups. Here, a large collection of hypothetical MTV-MOFs, which involve different combinations of –F, –NH<sub>2</sub>, and –OCH<sub>3</sub> groups, was computationally investigated to elucidate adsorption and membrane-based separation performances of materials for CF<sub>4</sub>/CH<sub>4</sub>, CH<sub>4</sub>/H<sub>2</sub>, CH<sub>4</sub>/N<sub>2</sub>, and N<sub>2</sub>/H<sub>2</sub> mixtures. This work features not only the extents of performances of MTV-MOFs based on their functional groups but also determines the most favorable linker/functional group combinations for the gas separations of interest. Results of this work can guide the future experimental efforts on MOFs with the identified favorable linker/functional group combinations and accelerate the design and discovery of optimal materials for similar gas separations.

## 1. Introduction

The hybrid nature of metal–organic frameworks (MOFs), originating from their inorganic and organic constituents, has sparked much interest in their use for gas adsorption

and separation,<sup>1,2</sup> catalysis,<sup>3</sup> sensing,<sup>4</sup> and drug delivery<sup>5</sup> applications. MOFs have various structural features that can be highly beneficial for gas separation such as high surface area and porosity, tunable pore size/shape, and linker functionalization.<sup>6,7</sup> Given the large number of organic linker and metal node combinations and promising performances of MOFs, there is an increasing trend of designing and/or testing MOFs.<sup>8–10</sup>

MOFs have been tested for a wide variety of gas separations involving carbon capture, noble gas separation, hydrocarbon separation *etc.*<sup>2</sup> Among them, CF<sub>4</sub>/CH<sub>4</sub> separation garnered less

Department of Chemical and Biological Engineering, Koc University, 34450

Istanbul, Turkey. E-mail: [hakdemir@ku.edu.tr](mailto:hakdemir@ku.edu.tr), [skeskin@ku.edu.tr](mailto:skeskin@ku.edu.tr)

† Electronic supplementary information (ESI) available. See DOI: <https://doi.org/10.1039/d2me00130f>



interest despite the industrial  $\text{CF}_4$  and  $\text{CH}_4$  emission into the atmosphere, high global warming potential of  $\text{CF}_4$  and its long atmospheric lifetime.<sup>11–13</sup> For example, Senkovska *et al.*<sup>12</sup> measured  $\text{CF}_4$  adsorption in several porous materials at ambient conditions and reported the largest  $\text{CF}_4$  uptake as 1.88 mol  $\text{kg}^{-1}$  in a MOF,  $\text{Zn}_4\text{O}(\text{dmcpz})_3$ . Calero *et al.*<sup>14</sup> predicted  $\text{CF}_4$  uptake in Cu-BTC to be around 1 mol  $\text{kg}^{-1}$  at ambient conditions using grand canonical Monte Carlo (GCMC) simulations. Our earlier work<sup>15</sup> focused on a collection of Zr-MOFs and reported  $\text{CF}_4/\text{CH}_4$  selectivity,  $\text{CF}_4$  working capacity, and  $\text{CF}_4$  regenerability to vary in the ranges of 0.8–6.2, 0.3–2.1 mol  $\text{kg}^{-1}$ , and 54.0–89.9%, respectively.

Due to the cleaner combustion characteristics of  $\text{CH}_4$  compared to gasoline and newly discovered reserves, it has become a more preferred energy source to reduce  $\text{CO}_2$  concentration in the air.<sup>16</sup> Similarly, the combustion of  $\text{H}_2$  ideally leads to no harmful emission whose widespread use can play a significant role in environmental remediation.<sup>17,18</sup> It is known that  $\text{CH}_4$  steam reforming and dry reforming lead to a gas mixture involving  $\text{CH}_4$  and  $\text{H}_2$ .<sup>19,20</sup> As the efficient separation of  $\text{CH}_4/\text{H}_2$  mixture can result in two sources of fuels that would be more preferable than the conventional fossil fuels, much research has been done on developing and identifying favorable materials for the  $\text{CH}_4/\text{H}_2$  separation.<sup>21,22</sup> High-throughput computational screening of 4350 and 4240 MOFs for adsorption and membrane-based separation of  $\text{CH}_4/\text{H}_2$  showed that MOFs can potentially have higher  $\text{CH}_4/\text{H}_2$  adsorption selectivity (up to 2028),  $\text{CH}_4$  working capacities (up to 7.3 mol  $\text{kg}^{-1}$ ),  $\text{CH}_4/\text{H}_2$  membrane selectivity (up to 713), and  $\text{CH}_4$  permeability (up to  $1.2 \times 10^8$  Barrer) than zeolites.<sup>23,24</sup>

$\text{CH}_4$  and  $\text{N}_2$  can co-exist in shale gases, natural gases, and landfill gases whose separation through conventional methods is energetically inefficient.<sup>25</sup>  $\text{CH}_4/\text{N}_2$  separation performances of MOFs have been experimentally probed in several studies and the ideal  $\text{CH}_4/\text{N}_2$  selectivities at ambient temperature were found to vary from 1.4 to 8.3.<sup>26–28</sup> Sumer *et al.*<sup>29</sup> screened more than 100 MOFs for  $\text{CH}_4/\text{N}_2$  separation and the best adsorbent was found to have a  $\text{CH}_4/\text{N}_2$  selectivity of 6.71 at 10 bar, 298 K, and  $\text{CH}_4$  working capacity of 3.64 mol  $\text{kg}^{-1}$  (between 10 and 1 bar). The top adsorbent has also been reported as one of the top materials for the membrane-based separation with a  $\text{CH}_4/\text{N}_2$  membrane selectivity of 10.26 and  $\text{CH}_4$  permeability of  $2.61 \times 10^6$  Barrer. Yan *et al.*<sup>30</sup> performed a high-throughput computational screening of >300 000 MOFs for separation of equimolar  $\text{CH}_4/\text{N}_2$  (50/50) separation at ambient conditions and the highest  $\text{CH}_4/\text{N}_2$  selectivity was reported as 29.5. Gulbalkan *et al.*<sup>31</sup> recently screened a large collection of MOFs and covalent-organic frameworks (COFs) composed of 5034 materials for  $\text{CH}_4/\text{N}_2$  separation at pressure-swing adsorption operation conditions and the highest  $\text{CH}_4/\text{N}_2$  selectivity was around 14.

$\text{N}_2/\text{H}_2$  separation is one of the less investigated gas separations while  $\text{N}_2$  and  $\text{H}_2$  uptakes of MOFs are more commonly reported. For instance, Mu *et al.*<sup>32</sup> synthesized UCMC-1 and obtained its maximum  $\text{H}_2$  storage capacity at

298 K, 26 bar as 3.4 mol  $\text{kg}^{-1}$  in addition to a  $\text{N}_2$  uptake of  $\sim 4$  mol  $\text{kg}^{-1}$  at 298 K, 25 bar. In an experimental study by Moreira *et al.*,<sup>16</sup> it has been shown that  $\text{UiO-66}(\text{Zr})-(\text{COOH})_2$  exhibits a higher affinity towards  $\text{N}_2$  than  $\text{H}_2$  at 269–373 K over a wide pressure range up to 30 bar ( $\text{N}_2/\text{H}_2$  ideal selectivity of  $\sim 8$  at 269 K, 20 bar). Regufe *et al.*<sup>33</sup> measured  $\text{N}_2$  and  $\text{H}_2$  adsorption in MIL-125(Ti)- $\text{NH}_2$  at 303 K from which it was concluded that  $\text{N}_2$  affinity of the material is greater than  $\text{H}_2$  affinity ( $\text{N}_2/\text{H}_2$  ideal selectivity of  $\sim 1.3$  at 303 K, 1 bar). Azar *et al.*<sup>34</sup> performed a large-scale computational screening of MOFs for adsorption-based  $\text{H}_2/\text{N}_2$  separation at ambient conditions and reported  $\text{H}_2/\text{N}_2$  selectivities of  $\sim 0.01$ –0.7 implying that all MOFs were  $\text{N}_2$  selective.

Many of the MOF studies in the literature focus on single-linker MOFs some of which have shown superior performances than conventional materials as outlined above. Besides single-linker MOFs, multivariate (MTV)-MOFs can also serve as efficient gas separation platforms as the combination of multiple functionalized linkers can lead to tailored gas affinities and significantly enhanced gas separation performances compared to pristine MOFs.<sup>35,36</sup> MTV-MOFs can be more selective than their counterparts with single type of functionalization. For instance, an MTV-MOF based on the functionalization of UiO-66 with  $-\text{NH}_2$  and  $-\text{F}_4$  groups has been predicted to have higher  $\text{CO}_2/\text{N}_2$  selectivities (26.3) than UiO-66 structures with solely  $-\text{NH}_2$  or  $-\text{F}_4$  functionalization (24.9 and 6.4).<sup>37</sup> Thus, unlocking the gas separation performance of MTV-MOFs for adsorption and membrane-based gas separations is highly desired.

In this work, MTV-MOFs<sup>38</sup> were computationally studied using a multi-stage screening procedure, mainly involving structural filtering and GCMC simulations, to investigate their potential for adsorption-based separation of  $\text{CF}_4/\text{CH}_4$ ,  $\text{CH}_4/\text{H}_2$ ,  $\text{CH}_4/\text{N}_2$ , and  $\text{N}_2/\text{H}_2$  mixtures. The investigated MTV-MOF database involves bare MOFs and their functionalized counterparts which may include up to three different functional groups ( $-\text{F}$ ,  $-\text{NH}_2$ ,  $-\text{OCH}_3$ ) constituting 16 subgroups of MTV-MOFs (*e.g.*,  $-\text{F}-\text{NH}_2-\text{OCH}_3$ ). For each MOF, gas uptakes were computed using GCMC simulations and these results were used to calculate adsorption selectivity, working capacity, and regenerability and based on the combination of these metrics, the top MOF adsorbents were identified. Besides, high-performing MOF adsorbents were further studied for membrane-based  $\text{CH}_4/\text{H}_2$  and  $\text{CH}_4/\text{N}_2$  separations. After identifying the top adsorbent and membranes materials for each gas separation, we examined structure-performance relations and discussed which combination of functional groups can lead to favorable adsorption and membrane-based separation performances of MOFs. As the subgroups of MTV-MOFs involve not only cases having two or three different functional groups but also linkers with identical functional groups, our results reveal the potential separation performance gains by grafting identical or disparate functional groups.



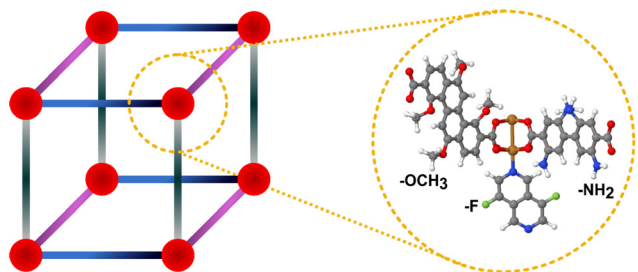


Fig. 1 Typical structures of MTV-MOFs probed (left) and a section of a representative MTV-MOF having three different functionalities (right) (different colourings of linkers on the left designate different linkers which may have different functional groups. Atom colouring: gray: C, red: O, brown: Cu, green: F, white: H, blue: N).

## 2. Computational methods

In this work, we focused on the MTV-MOF database<sup>38</sup> (based on copper paddlewheel nodes and pcu topology) involving 560 parent/bare MOFs (structures originally named as pMOFs) and 10995 functionalized MOFs (structures originally named as cuf MOFs). The functionalized MOFs may include  $-F$ ,  $-NH_2$ , and/or  $-OCH_3$  functional groups. Fig. 1 demonstrates the general structures of MTV-MOFs as well as an example MTV-MOF where each linker involves different functional group ( $-F$ ,  $-NH_2$  and  $-OCH_3$ ). The textural properties of 11129 MOFs (GCD (global cavity diameter), PLD (pore limiting diameter), LCD (largest cavity diameter), surface area, probe-occupiable void fraction, probe-occupiable pore volume) were calculated with a probe radius of 1.84 Å using Zeo++.<sup>39,40</sup> Note that GCD is the largest pore size in the material which may not be found in the pore

channel where PLD and LCD are located.<sup>41</sup> Fig. 2 demonstrates the structural property distributions of all MTV-MOFs except those having too close interatomic distances (*i.e.*, interatomic distances less than 0.9 Å). It can be inferred that the MTV-MOF database involves structurally diverse structures where bare MOFs are somewhat more porous than their functionalized counterparts. The PLD distribution curves overlap in a large range of values while the discrepancies in surface area, void fraction, and pore volume distributions are considerably larger.

MOFs that satisfy the following criteria were kept for further molecular simulations to eliminate potential structural accessibility, structural integrity, and practical use problems: (1) MOFs shall have non-zero accessible surface areas and PLDs larger than sizes of adsorbates that are of interest ensuring structural accessibility. (2) Interatomic distances in MOFs shall be larger than 0.9 Å to avoid structures with atomic overlaps or too close atoms. (3) Working capacities, the differences between gas uptakes computed at adsorption and desorption conditions, shall be positive to have practical use of MOFs in pressure/vacuum swing adsorption operations. After applying these criteria, we ended up with 11035, 11115, 11115, and 11116 different MOFs for the separation of  $CF_4/CH_4$ ,  $CH_4/H_2$ ,  $CH_4/N_2$ , and  $N_2/H_2$  mixtures.

Adsorption of  $CF_4/CH_4$ ,  $CH_4/H_2$ ,  $CH_4/N_2$ , and  $N_2/H_2$  mixtures in MTV MOFs was investigated using GCMC simulations and diffusion of  $CH_4/H_2$  and  $CH_4/N_2$  mixtures in MTV-MOFs were studied by molecular dynamics (MD) simulations in RASPA, respectively.<sup>42</sup> Bulk compositions of these gas mixtures were determined such that they have industrial relevance and/or enable benchmark with other

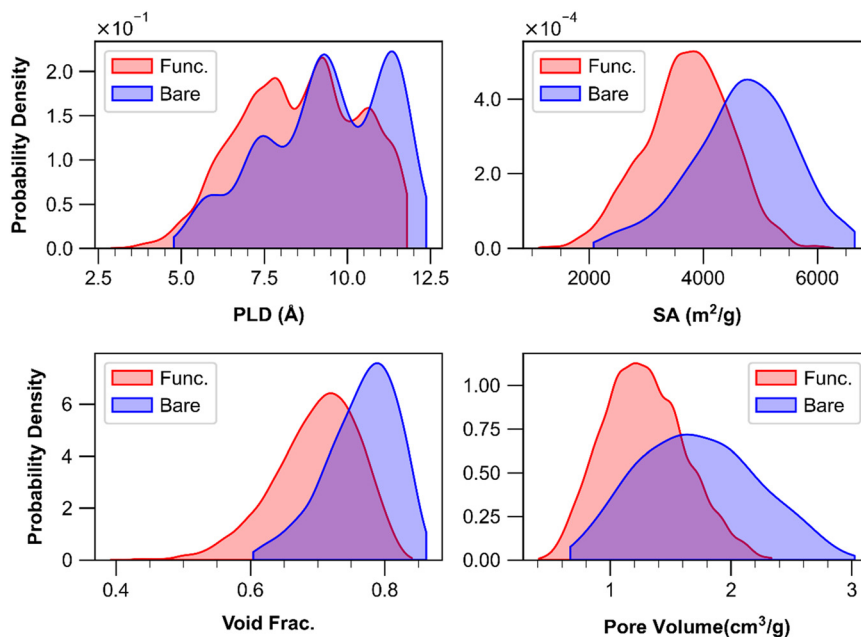


Fig. 2 Kernel density plots showing distribution of structural properties of 11129 MTV-MOFs where bare and functionalized (Func.) MOFs were shown separately.



literature studies.<sup>24,31,43,44</sup> For instance, CF<sub>4</sub> removal from CH<sub>4</sub> constitutes a significant stage of reducing greenhouse gas concentration in the air.<sup>15</sup> As these two sorbates have similar properties, finding sorbents that can achieve efficient CF<sub>4</sub>/CH<sub>4</sub> separation is crucial. While a large variety of gas compositions has been studied earlier for CF<sub>4</sub>/CH<sub>4</sub> separation,<sup>43</sup> we preferred an equimolar mixture to be able to benchmark the results of this work with our earlier work<sup>15</sup> which was possibly the largest MOF screening work in terms of CF<sub>4</sub>/CH<sub>4</sub> separation. H<sub>2</sub> or N<sub>2</sub> removal from CH<sub>4</sub> is highly important in the context of natural gas separation for which equimolar binary mixtures are typically used.<sup>31,45</sup> Similarly, improving the efficiency of N<sub>2</sub>/H<sub>2</sub> separation bears importance for the processes of carbon black manufacturing, and ammonia synthesis.<sup>46,47</sup> N<sub>2</sub>/H<sub>2</sub> composition is selected based on former experimental and computational studies.<sup>34,48</sup> These gas compositions and pressures were listed in Table S1† together with total simulation cycles for GCMC. All GCMC simulations were carried out at 298 K. In all GCMC simulations, the number of equilibration and production cycles were equal. The following types of moves were employed with equal probability: insertion/deletion, translation, rotation (only for N<sub>2</sub>), and molecule identity change. MOF atoms were assigned Universal Force Field (UFF<sup>49</sup>) parameters and partial atomic charges in metal-organic frameworks (PACMOF<sup>50</sup>) charges. The interaction parameters for the gas molecules were obtained from the literature which are available in Table S2.†<sup>51–54</sup> The Lennard–Jones interactions were cutoff at 12 Å and electrostatic calculations were performed (only for N<sub>2</sub>) using Ewald summation method.<sup>55</sup>

Results of GCMC simulations, the adsorbed gas amounts ( $N_i$ ), were used to compute the adsorption-based gas separation performances of MOFs: the adsorption selectivity is defined as  $S_{\text{ads},1/2} = \frac{N_1/N_2}{y_1/y_2}$  where  $N$  and  $y$  designate the adsorption amount and the mole fraction of a gas component in the mixture. Working capacity is mathematically expressed as  $\Delta N_1 = N_{\text{ads},1} - \Delta N_{\text{des},1}$  where the first and second term on the right-hand side represent gas uptakes computed from GCMC simulations at the adsorption and desorption conditions. Regenerability of an adsorbent is calculated as  $R = \frac{\Delta N_1}{N_{\text{ads},1}} \times 100$ .<sup>66</sup> Since all of these metrics, selectivity, working capacity and regenerability, are important to identify the most promising MOF adsorbents, we defined the Score <sub>$X,i$</sub>  =  $\frac{X_i}{X_{\text{max}}} \times 100$ , where  $X_i$  and  $X_{\text{max}}$  denote the value of the individual performance metric  $X$  (selectivity/working capacity/regenerability) for material  $i$  and the highest value of the individual performance metric  $X$  across all materials, respectively. The individual separation performance scores were summed to determine the overall separation performance scores of MOFs and the materials with the highest overall separation performances were assigned the highest adsorbent rankings.

For the top materials identified for each gas separation, MD simulations were performed in the NVT ensemble at 298 K using a Nose–Hoover thermostat.<sup>56</sup> In these simulations, 10<sup>5</sup> initialization, 10<sup>6</sup> equilibration, and 15 × 10<sup>6</sup> production

steps (time step of 1 fs) were used where the number of gas molecules (gas loading) employed relies on GCMC simulation results at adsorption conditions. Self-diffusivities of gases in  $x$ ,  $y$ , and  $z$  directions were determined using Einstein's relation at long simulation times.<sup>57</sup> Self-diffusivities in a particular direction that were much lower (*e.g.*, two orders of magnitude smaller) than other self-diffusivities in other directions were discarded in the calculation of average self-diffusivity calculation ( $D_{\text{self},i} = \frac{D_{\text{self},i,x} + D_{\text{self},i,y} + D_{\text{self},i,z}}{3}$ ). In such cases, the dimensionality of the system in Einstein's relation was adjusted accordingly. The self-diffusivities are averaged over five simulations. Combining the results of GCMC and MD simulations, gas permeabilities were calculated as  $P_i = \frac{c_i \times D_{\text{self},i}}{f_i}$  where  $c_i$ ,  $D_{\text{self},i}$ , and  $f_i$  represent the gas concentration at the feed side, self-diffusivity of gas, and feed side fugacity of the gas species  $i$ , respectively. The diffusion selectivity and membrane selectivity (component 1 over 2) are defined as  $S_{\text{diff},12} = \frac{D_{\text{self},1}}{D_{\text{self},2}}$  and  $S_{\text{mem},12} = S_{\text{ads},12} \times S_{\text{diff},12}$ , successively.<sup>66</sup>

## 3. Results & discussion

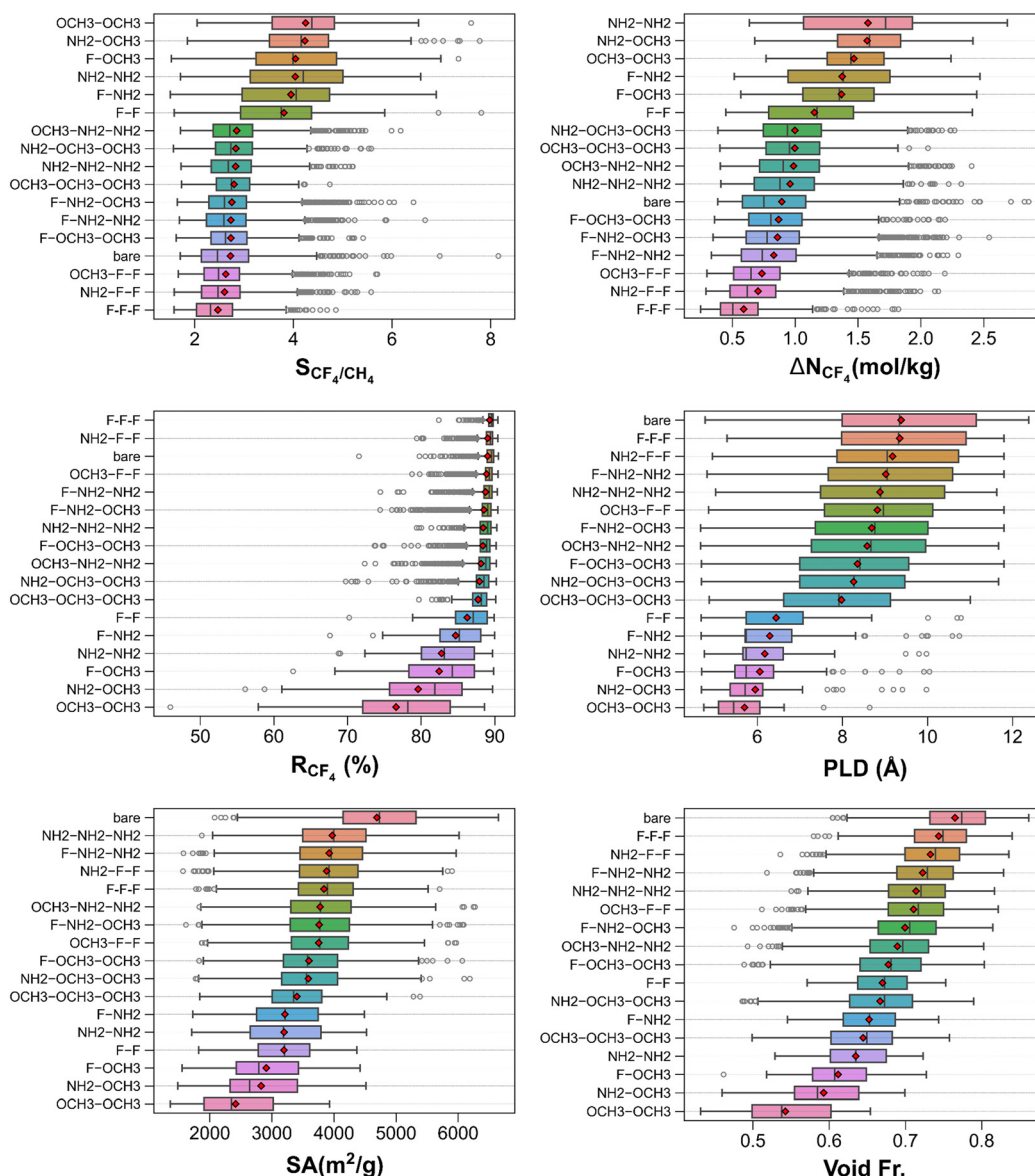
### 3.1 CF<sub>4</sub>/CH<sub>4</sub> separation

Fig. S1† delineates the CF<sub>4</sub>/CH<sub>4</sub> separation performance metrics of 11 035 MOFs as well as their pore features. The top left panel shows CF<sub>4</sub>/CH<sub>4</sub> selectivity, CF<sub>4</sub> working capacity, and CF<sub>4</sub> regenerability of the MOFs which were calculated as 1.4–8.2, 0.2–2.9 mol kg<sup>-1</sup>, and 45.9–90.5%, respectively. The three most CF<sub>4</sub> selective MOFs (pMOF\_10, cuf\_3865, and cuf\_8464) exhibit CF<sub>4</sub>/CH<sub>4</sub> selectivities of 8.2, 7.8, and 7.8, CF<sub>4</sub> working capacities of 2.9, 2.4, and 1.6 mol kg<sup>-1</sup>, and CF<sub>4</sub> regenerabilities of 71.6, 70.2, and 64.9%, respectively. The top right panel shows that there is a group of highly porous MOFs (void fraction mostly >0.7) located in the relatively low CF<sub>4</sub>/CH<sub>4</sub> selectivity (<4) and CF<sub>4</sub> working capacity range (<1 mol kg<sup>-1</sup>). In contrast, MOFs with the highest CF<sub>4</sub>/CH<sub>4</sub> selectivity and CF<sub>4</sub> working capacity possess medium-high void fractions (~0.46–0.68). The bottom left panel exhibits that the most CF<sub>4</sub> selective MOFs have PLDs of ~6 Å. However, there are also MOFs with similar PLDs attaining very low selectivities (<2). The bottom right panel illustrates that the largest CF<sub>4</sub>/CH<sub>4</sub> selectivities are located around 2000 m<sup>2</sup> g<sup>-1</sup> whereas the smallest CF<sub>4</sub>/CH<sub>4</sub> selectivities are obtained by MOFs with very large surface areas (>5000 m<sup>2</sup> g<sup>-1</sup>). All in all, these results suggest that MTV-MOFs that are not overly porous (*i.e.*, PLDs <7 Å, surface areas <3000 m<sup>2</sup> g<sup>-1</sup>) can attain high adsorption-based CF<sub>4</sub>/CH<sub>4</sub> separation performances in terms of selectivity, working capacity, and regenerability.

Fig. 3 shows the breakdown of CF<sub>4</sub>/CH<sub>4</sub> separation performance metrics and textural features of MOFs into functional groups. The top left panel exhibits that, on average, MOFs having linkers functionalized with –OCH<sub>3</sub> groups (specifically, –OCH<sub>3</sub>–OCH<sub>3</sub>, meaning two linkers are functionalized with –OCH<sub>3</sub> group) are the most CF<sub>4</sub> selective. On the contrary, those functionalized with –F groups (*i.e.*, –F–







**Fig. 3**  $\text{CF}_4/\text{CH}_4$  separation performance metrics of MTV MOFs and their pore features categorized by their functional groups. In all box-and-whisker plots, MOF groups are sorted from top to bottom by mean values in descending order where mean values are shown with red diamonds. Boxes show the range of values between the first and third quartile while the whiskers designate the distribution of other data points except outliers. Outliers are denoted as empty circles which are defined as data points away from either end of the boxes by more than 1.5 interquartile range.

F-F) are the least  $\text{CF}_4$  selective. Bare MOFs is one of the groups showing large variations in selectivity from 1.7 up to 8.2. In general, the lowest  $\text{CF}_4/\text{CH}_4$  selectivity obtained in each group is very close to each other suggesting that there are cases where the selectivity of the bare MOFs may not be simply improved through functionalization. The top right panel depicts that MOFs functionalized with  $-\text{NH}_2-\text{NH}_2$  (F-F-F) groups attain the largest (smallest) mean  $\text{CF}_4$  working capacities. As a group, bare MOFs attain one of the low mean  $\text{CF}_4$  working capacities ( $\sim 0.9 \text{ mol kg}^{-1}$ ), however, some MOFs among them can demonstrate quite high working capacities as exemplified by pMOF\_10 with the highest  $\text{CF}_4$  working capacity of  $2.9 \text{ mol kg}^{-1}$ . The middle-left panel illustrates that many groups of MOFs (going from top to bottom, F-F-F to

$-\text{OCH}_3-\text{OCH}_3-\text{OCH}_3$ ) show high  $\text{CF}_4$  regenerabilities ( $>85\%$ ). In contrast, MOFs functionalized with  $-\text{OCH}_3-\text{OCH}_3$  and  $-\text{NH}_2-\text{OCH}_3$  groups acquire the lowest mean  $\text{CF}_4$  regenerabilities ( $<80\%$ ). Overall, these observations imply that by combining multiple functional groups,  $\text{CF}_4/\text{CH}_4$  separation performance metrics of MOFs can be drastically altered. However, this does not guarantee that multifunctional MOFs can always perform better than all bare MOFs in terms of a particular separation performance metric.

Since the grafting of functional groups can block portions of the pores or create new surfaces, the textural properties of bare and functionalized MOFs are benchmarked to see if there are clear pore feature trends across different groups of



MOFs. As the middle right panel demonstrates, several categories of MOFs (bare MOFs, MOFs functionalized with  $-F$ ,  $-F-F$  and  $-NH_2-F-F$  groups) possess very similar and high PLDs on average. The smallest PLDs belong to MOFs that are functionalized with  $-OCH_3-OCH_3$  groups. The bottom panels show that the bare MOFs possess the highest mean surface area and void fraction whereas MOFs functionalized with  $-OCH_3-OCH_3$  groups have the lowest mean surface areas, in line with the PLD trends.

Unlike the traditional approach of ranking materials solely based on adsorption selectivities, here, we evaluated MOF adsorbents using multiple metrics (*i.e.*, adsorption selectivity, working capacity, and regenerability). Table S3† enumerates the 20 best performing MOFs identified for adsorption-based separation of  $CF_4/CH_4$  mixture. These MOFs are dominantly

functionalized MOFs (16 out of 20), yet the top three MOFs are all bare MOFs (pMOF\_10, pMOF\_26, and pMOF\_8) with  $CF_4/CH_4$  selectivities of 6.0–8.2,  $CF_4$  working capacities of 2.7–2.9 mol  $kg^{-1}$ , and  $CF_4$  regenerabilities of 71.6–80.6%. Considering the number of occurrences in the top 20 list,  $-F-NH_2$  functionalization is one of the cases which achieve favorable  $CF_4/CH_4$  separation features. It is noteworthy that most of these top MOFs possess narrow pores ( $\sim 5-7$  Å) with surface areas of 1824.7–3724.8  $m^2 g^{-1}$ , void fractions of 0.496–0.657, and pore volumes of 0.574–0.941  $cm^3 g^{-1}$ .

### 3.2 $CH_4/H_2$ separation

Fig. S2† shows  $CH_4/H_2$  separation performance metrics of the MOFs together with their textural properties. As the top left

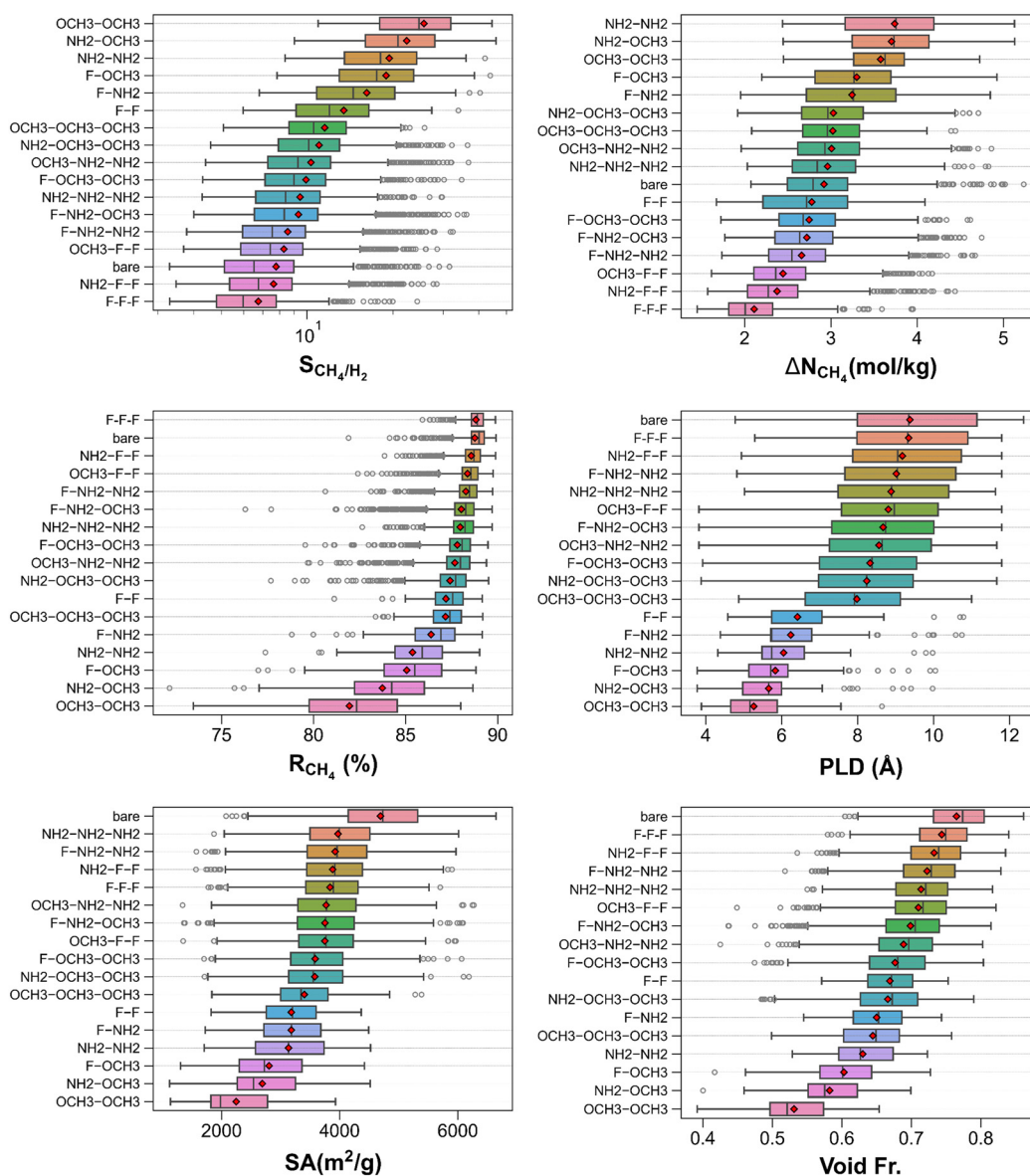


Fig. 4  $CH_4/H_2$  separation performance metrics and structural properties of MOFs classified by their functional groups.



panel demonstrates, most of the MOFs are highly regenerable ( $\text{CH}_4$  regenerability  $>85\%$ ).  $\text{CH}_4/\text{H}_2$  selectivity and  $\text{CH}_4$  working capacity of the MOFs span the ranges of 3.3–46.0, and 1.5–5.2 mol  $\text{kg}^{-1}$ , respectively. The top right panel exhibits that more  $\text{CH}_4$  selective MOFs tend to be denser than less  $\text{CH}_4$  selective ones. Interestingly, the most porous structures (void fraction  $\geq 0.85$ ) attain limited  $\text{CH}_4$  working capacities ( $<2.4$  mol  $\text{kg}^{-1}$ ) whereas MOFs with the largest  $\text{CH}_4$  working capacities possess medium-high void fractions (0.56–0.67). The bottom panels illustrate the clear inverse  $\text{CH}_4/\text{H}_2$  selectivity vs. PLD and  $\text{CH}_4/\text{H}_2$  selectivity vs. surface area trends where the highest selectivities are attained around PLDs of 4–6 Å and surface areas of  $\sim 1200$ – $2200$   $\text{m}^2$   $\text{g}^{-1}$ . Since both adsorbates interact with the framework through dispersion forces only, these inverse trends hint the significantly reduced dispersion effects as the structure become more porous. Thus, superior  $\text{CH}_4/\text{H}_2$  separation performances are more likely to be found in MTV-MOFs with relatively small pores and porosities.

Fig. 4 displays the classification of the  $\text{CH}_4/\text{H}_2$  separation performance metrics and structural features of the MOFs by functional groups. The top left panel shows that the most (least)  $\text{CH}_4$  selective MOFs are  $-\text{OCH}_3$ – $\text{OCH}_3$  ( $-\text{F}$ – $\text{F}$ ) functionalized MOFs on average. While bare MOFs tend to have lower  $\text{CH}_4/\text{H}_2$  selectivities than some of the functionalized MOF groups (such as  $-\text{OCH}_3$ – $\text{OCH}_3$ ,  $-\text{NH}_2$ – $\text{OCH}_3$ , and  $-\text{NH}_2$ – $\text{NH}_2$ ), some of the bare MOFs can have high  $\text{CH}_4/\text{H}_2$  selectivities (up to  $\sim 32$ ), comparable with most of the functionalized MOFs. The top right panel exhibits that both bare and functionalized MOFs can span large ranges of  $\text{CH}_4$  working capacities. Interestingly, the largest  $\text{CH}_4$  working capacities are obtained by the MOFs functionalized with three functional groups (*i.e.*,  $-\text{OCH}_3$ – $\text{NH}_2$ – $\text{NH}_2$ , and  $-\text{NH}_2$ – $\text{NH}_2$ – $\text{NH}_2$ ) despite reduced space for adsorption. The

middle-left panel shows that many groups of MOFs exhibit similar  $\text{CH}_4$  regenerabilities on average ( $>85\%$ ) while those functionalized with  $-\text{OCH}_3$ – $\text{OCH}_3$  have the most dissimilar mean  $\text{CH}_4$  regenerability ( $\sim 82\%$ ), being the lowest. Considering all above, it can be inferred that addition of multiple functional groups modifies the pore structures dramatically which in turn can bring about significantly different  $\text{CH}_4/\text{H}_2$  adsorption-based separation performances.

Table 1 lists the top 20 MOFs identified for  $\text{CH}_4/\text{H}_2$  separation and they are all found to be functionalized structures. The best three MOFs are *cuf*\_2878, *cuf*\_824, and *cuf*\_818 with  $\text{CH}_4/\text{H}_2$  selectivities of 42.1, 46.0, and 43.9,  $\text{CH}_4$  working capacities of 5.1, 4.6, and 4.6 mol  $\text{kg}^{-1}$ , and  $\text{CH}_4$  regenerabilities of 80.3, 76.2, and 77.5%, respectively. As many other materials in the top 20 list are, these top materials are also functionalized with  $-\text{NH}_2$  group (*i.e.*,  $-\text{NH}_2$ – $\text{OCH}_3$ ,  $-\text{OCH}_3$ – $\text{NH}_2$ – $\text{NH}_2$ , and  $-\text{NH}_2$ – $\text{NH}_2$ , respectively) (see Table S4†). Considering the ranges of PLD (3.94–6.37 Å), surface area (1136.1–2543.9  $\text{m}^2$   $\text{g}^{-1}$ ), void fraction (0.437–0.581), and pore volume (0.455–0.712  $\text{cm}^3$   $\text{g}^{-1}$ ), the top 20 MOFs can be regarded as moderately porous structures (see Table S4†).

While porous materials can serve as adsorbents in separation processes, they can also act as efficient membranes as long as adsorbates diffuse fast enough through the pores of the material. It is known that the computational cost of obtaining membrane-based performances is much higher than that of adsorption-based performances.<sup>67</sup> Thus, we chose only two cases ( $\text{CH}_4/\text{H}_2$  and  $\text{CH}_4/\text{N}_2$ ), which are the most commonly studied cases among all four cases, to investigate membrane-based separation. To reveal the potential of MTV-MOFs as membranes, MD calculations were performed for the top 20 adsorbents to compute the diffusion of  $\text{CH}_4/\text{H}_2$  and  $\text{CH}_4/\text{N}_2$  mixture in the pores. As expected,  $\text{H}_2$  diffuses faster than  $\text{CH}_4$

**Table 1** 20 best performing MOF adsorbents for the  $\text{CH}_4/\text{H}_2$  separation together with their membrane-based separation performances

| Structure        | $S_{\text{ads},\text{CH}_4/\text{H}_2}$ | $\Delta N_{\text{CH}_4}$<br>(mol $\text{kg}^{-1}$ ) | $R_{\text{CH}_4}$ (%) | $S_{\text{diff},\text{CH}_4/\text{H}_2}$ | $S_{\text{mem},\text{CH}_4/\text{H}_2}$ | $D_{\text{self},\text{CH}_4}$ ( $\text{m}^2$ $\text{s}^{-1}$ ) | $D_{\text{self},\text{H}_2}$ ( $\text{m}^2$ $\text{s}^{-1}$ ) | $P_{\text{CH}_4}$ (Barrer) | $P_{\text{H}_2}$ (Barrer) |
|------------------|---|---|-----------------------|--|---|--|---|----------------------------|---------------------------|
| <i>cuf</i> _2878 | 42.1                                    | 5.1   | 80.3                  | 0.24                                     | 10.0                                    | $1.40 \times 10^{-8}$  | $5.92 \times 10^{-8}$   | $4.77 \times 10^5$         | $4.67 \times 10^4$        |
| <i>cuf</i> _824  | 46.0                                    | 4.6   | 76.2                  | 0.24                                     | 10.9                                    | $1.24 \times 10^{-8}$  | $5.22 \times 10^{-8}$   | $4.27 \times 10^5$         | $3.83 \times 10^4$        |
| <i>cuf</i> _818  | 43.9                                    | 4.6   | 77.5                  | 0.28                                     | 12.2                                    | $1.98 \times 10^{-8}$  | $7.13 \times 10^{-8}$   | $6.78 \times 10^5$         | $5.44 \times 10^4$        |
| <i>cuf</i> _586  | 37.8                                    | 5.0   | 80.2                  | 0.27                                     | 10.2                                    | $1.15 \times 10^{-8}$  | $4.27 \times 10^{-8}$   | $3.82 \times 10^5$         | $3.65 \times 10^4$        |
| <i>cuf</i> _110  | 42.2                                    | 4.7   | 75.2                  | 0.15                                     | 6.2                                     | $5.25 \times 10^{-9}$  | $3.59 \times 10^{-8}$   | $1.75 \times 10^5$         | $2.77 \times 10^4$        |
| <i>cuf</i> _3153 | 42.3                                    | 4.5   | 78.5                  | 0.18                                     | 7.5                                     | $3.86 \times 10^{-9}$  | $2.19 \times 10^{-8}$   | $1.24 \times 10^5$         | $1.62 \times 10^4$        |
| <i>cuf</i> _1627 | 38.2                                    | 4.7   | 81.9                  | 0.29                                     | 11.2                                    | $1.77 \times 10^{-8}$  | $6.03 \times 10^{-8}$   | $5.55 \times 10^5$         | $4.82 \times 10^4$        |
| <i>cuf</i> _2872 | 37.1                                    | 4.8   | 81.2                  | 0.29                                     | 10.7                                    | $2.23 \times 10^{-8}$  | $7.73 \times 10^{-8}$   | $7.11 \times 10^5$         | $6.49 \times 10^4$        |
| <i>cuf</i> _7134 | 42.6                                    | 4.3   | 78.8                  | 0.29                                     | 12.4                                    | $1.22 \times 10^{-8}$  | $4.20 \times 10^{-8}$   | $3.89 \times 10^5$         | $3.07 \times 10^4$        |
| <i>cuf</i> _1633 | 39.1                                    | 4.5   | 79.9                  | 0.24                                     | 9.4                                     | $1.22 \times 10^{-8}$  | $5.11 \times 10^{-8}$   | $3.77 \times 10^5$         | $3.93 \times 10^4$        |
| <i>cuf</i> _3160 | 38.7                                    | 4.5   | 80.7                  | 0.18                                     | 7.1                                     | $4.54 \times 10^{-9}$  | $2.47 \times 10^{-8}$   | $1.44 \times 10^5$         | $1.99 \times 10^4$        |
| <i>cuf</i> _3866 | 40.4                                    | 4.4   | 78.8                  | 0.34                                     | 13.6                                    | $2.07 \times 10^{-8}$  | $6.15 \times 10^{-8}$   | $6.97 \times 10^5$         | $4.99 \times 10^4$        |
| <i>cuf</i> _2640 | 32.8                                    | 5.0   | 81.3                  | 0.25                                     | 8.3                                     | $1.47 \times 10^{-8}$  | $5.82 \times 10^{-8}$   | $4.50 \times 10^5$         | $5.28 \times 10^4$        |
| <i>cuf</i> _810  | 36.5                                    | 4.6   | 80.9                  | 0.21                                     | 7.6                                     | $7.98 \times 10^{-9}$  | $3.84 \times 10^{-8}$   | $2.52 \times 10^5$         | $3.24 \times 10^4$        |
| <i>cuf</i> _2160 | 35.1                                    | 4.9   | 78.9                  | 0.11                                     | 3.8                                     | $4.87 \times 10^{-9}$  | $4.54 \times 10^{-8}$   | $1.51 \times 10^5$         | $3.90 \times 10^4$        |
| <i>cuf</i> _533  | 35.0                                    | 4.7   | 80.9                  | 0.24                                     | 8.4                                     | $1.88 \times 10^{-8}$  | $7.84 \times 10^{-8}$   | $5.90 \times 10^5$         | $6.85 \times 10^4$        |
| <i>cuf</i> _811  | 34.8                                    | 4.6   | 82.1                  | 0.21                                     | 7.3                                     | $1.13 \times 10^{-8}$  | $5.37 \times 10^{-8}$   | $3.52 \times 10^5$         | $4.69 \times 10^4$        |
| <i>cuf</i> _3143 | 44.5                                    | 3.8   | 75.0                  | 0.10                                     | 4.3                                     | $1.30 \times 10^{-9}$  | $1.34 \times 10^{-8}$   | $3.89 \times 10^4$         | $8.75 \times 10^3$        |
| <i>cuf</i> _812  | 42.1                                    | 4.0   | 75.9                  | 0.13                                     | 5.6                                     | $4.54 \times 10^{-9}$  | $3.43 \times 10^{-8}$   | $1.43 \times 10^5$         | $2.51 \times 10^4$        |
| <i>cuf</i> _9626 | 34.3                                    | 4.6   | 81.6                  | 0.24                                     | 8.2                                     | $9.41 \times 10^{-9}$  | $3.92 \times 10^{-8}$   | $2.91 \times 10^5$         | $3.45 \times 10^4$        |



since it has weaker interaction with the MOF atoms compared to  $\text{CH}_4$  in addition to being lighter and smaller. This leads to  $\text{CH}_4/\text{H}_2$  diffusion selectivities that are considerably smaller than unity for all the MTV-MOFs that we studied by MD. Combining the low diffusion selectivities toward  $\text{CH}_4$  with the high adsorption selectivities lead to membranes offering  $\text{CH}_4/\text{H}_2$  membrane selectivities in the range of  $\sim 4$ –14. Weighing  $\text{CH}_4/\text{H}_2$  membrane selectivity and  $\text{CH}_4$  permeability equally for identifying the best membrane materials, *cuf\_3866* (F-NH<sub>2</sub> functionalized), *cuf\_818* (F-OCH<sub>3</sub> functionalized), and *cuf\_2872* (F-NH<sub>2</sub> functionalized) were found to be the ideal candidates for the selective  $\text{CH}_4$  removal from  $\text{H}_2$  with  $\text{CH}_4/\text{H}_2$  membrane selectivities of 10.7–13.6 and  $\text{CH}_4$  permeabilities of  $6.78 \times 10^5$ – $7.11 \times 10^5$  Barrer.  $\text{CH}_4$  permeabilities are generally about one order of magnitude larger than  $\text{H}_2$  permeabilities which is largely due to the stronger adsorption of  $\text{CH}_4$  compared to  $\text{H}_2$  (higher concentrations of  $\text{CH}_4$  in the membrane).

### 3.3 $\text{CH}_4/\text{N}_2$ separation

Fig. S3† delineates the  $\text{CH}_4/\text{N}_2$  separation performance metrics of the MOFs along with their textural properties. The top left panel demonstrates that the  $\text{CH}_4/\text{N}_2$  selectivities,  $\text{CH}_4$  working capacities, and  $\text{CH}_4$  regenerabilities cover the ranges of 1.4–5.2, 1.4–4.8 mol kg<sup>-1</sup>, and 69.9–89.7%, respectively. While the two most  $\text{CH}_4$  selective MOFs can attain somewhat higher  $\text{CH}_4/\text{N}_2$  selectivities ( $>5$ ) than the rest of the material set, they suffer from relatively low regenerability ( $<75\%$ ), signifying a trade-off between the selectivity and reusability of materials. The top right panel shows that high  $\text{CH}_4/\text{N}_2$  selectivities ( $>4$ ) are seen in moderately porous structures (void fraction of 0.392–0.636) while the most porous structures (void fraction  $>0.84$ ) can acquire  $\text{CH}_4/\text{N}_2$  selectivities up to 1.7 and  $\text{CH}_4$  working capacities up to 2.3 mol kg<sup>-1</sup>. The bottom panels reveal that the biggest spreads

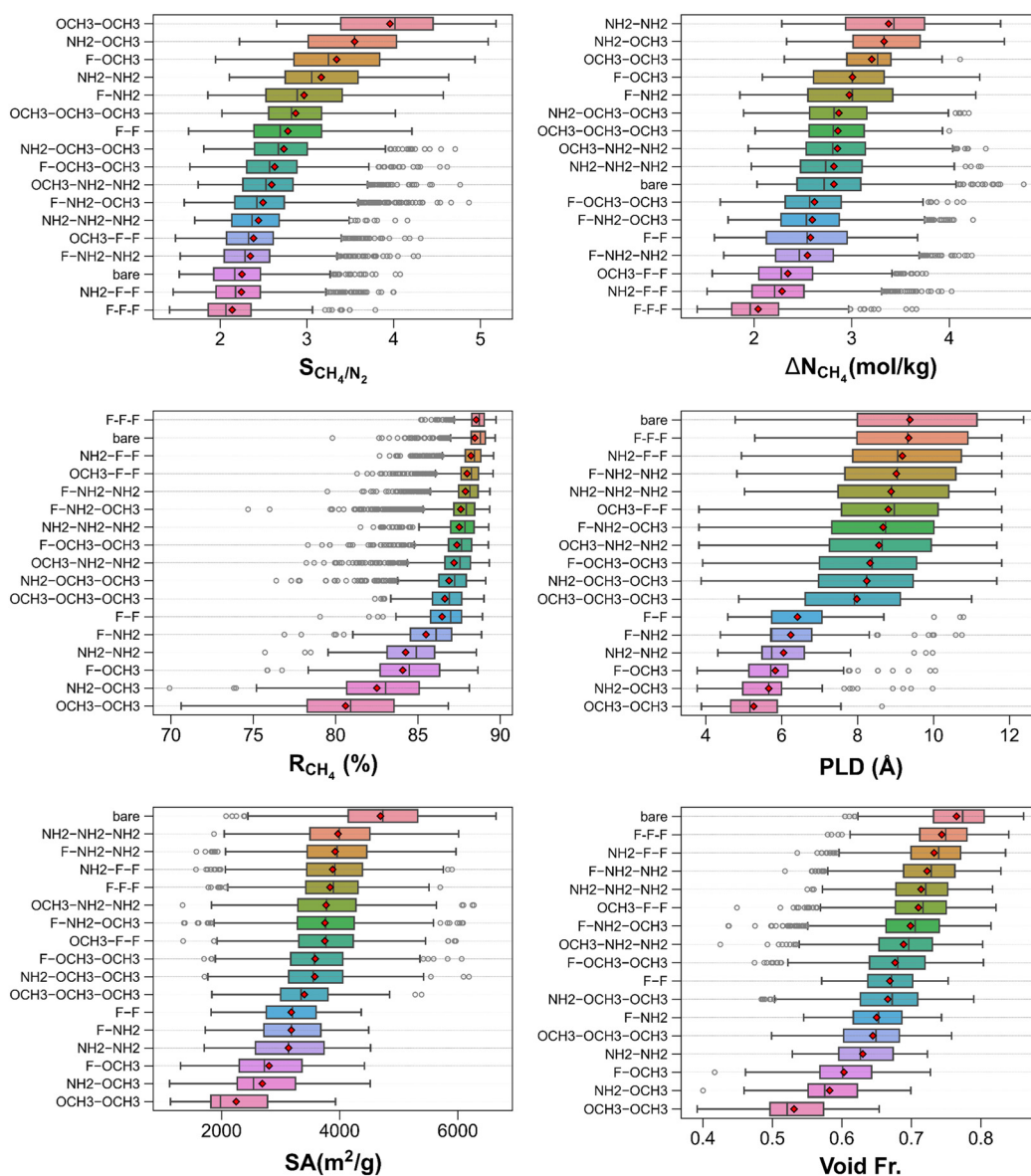


Fig. 5 Breakdown of  $\text{CH}_4/\text{N}_2$  separation performance metrics and textural properties of MOFs.





in CH<sub>4</sub>/N<sub>2</sub> selectivity are observed at relatively low PLDs (~6 Å) and surface areas (~2000 m<sup>2</sup> g<sup>-1</sup>) beyond which selectivities start converging to 2–3. Comparing Fig. S2 and S3,† it can be deduced that the separation performances trends seen for the CH<sub>4</sub>/H<sub>2</sub> and CH<sub>4</sub>/N<sub>2</sub> adsorption-based separation are very similar to each other albeit MTV-MOFs having smaller CH<sub>4</sub>/N<sub>2</sub> adsorption selectivities as N<sub>2</sub>, having a quadrupole moment, interacts slightly stronger than H<sub>2</sub>.

Fig. 5 displays the categorized (by functional groups) CH<sub>4</sub>/N<sub>2</sub> separation performance metrics and textural properties of MOFs. The top left panel shows that while –NH<sub>2</sub>–OCH<sub>3</sub> and –F–OCH<sub>3</sub> functionalized MOFs can achieve large CH<sub>4</sub>/N<sub>2</sub> selectivities, the highest mean CH<sub>4</sub>/N<sub>2</sub> selectivities are obtained by the MOFs functionalized with –OCH<sub>3</sub>–OCH<sub>3</sub>. The mean CH<sub>4</sub>/N<sub>2</sub> selectivity of bare MOFs is one of the lowest of all groups below which MOFs functionalized with –NH<sub>2</sub>–F–F and –F–F–F are located with slightly lower mean selectivities. The top right panel demonstrates that the largest (smallest) mean CH<sub>4</sub> working capacity is attained by MOFs functionalized with –NH<sub>2</sub>–NH<sub>2</sub> (–F–F–F). However, the largest CH<sub>4</sub> working capacity was observed in a bare MOF. The middle-left panel manifests that many functionalized MOF groups (*e.g.*, –F–F–F, –NH<sub>2</sub>–F–F, –OCH<sub>3</sub>–F–F *etc.*) and bare MOFs acquire similarly high CH<sub>4</sub> regenerabilities on average (>85%) while MOFs functionalized with –OCH<sub>3</sub>–OCH<sub>3</sub> have the least mean CH<sub>4</sub> regenerability (~80%) which is comparable with the former.

In Table 2, 20 best performing MOFs for CH<sub>4</sub>/N<sub>2</sub> separation are tabulated where CH<sub>4</sub>/N<sub>2</sub> selectivities, CH<sub>4</sub> working capacities, and CH<sub>4</sub> regenerabilities span the ranges of 3.5–5.0, 3.8–4.8 mol kg<sup>-1</sup>, and 73.0–84.6%, respectively. These MOFs are moderately porous structures with PLDs of 4.09–11.39 Å, surface areas of 1868.0–3277.6 m<sup>2</sup> g<sup>-1</sup>, void fractions of 0.514–0.650, and pore volumes of 0.557–0.937 cm<sup>3</sup> g<sup>-1</sup> (see

Table S5†). Among the top 20 MOFs, which are all functionalized MOFs, the top three MOFs (cuf\_2878, cuf\_1627, and cuf\_586) are functionalized with –F, –OCH<sub>3</sub> and –NH<sub>2</sub> groups (*i.e.*, –NH<sub>2</sub>–NH<sub>2</sub>, –F–OCH<sub>3</sub>, and –NH<sub>2</sub>–OCH<sub>3</sub>, successively) (see Table S5†). While they attain moderate-high selectivities (4.6, 4.7, and 4.5), they exhibit large CH<sub>4</sub> working capacities (4.5, 4.2, and 4.4 mol kg<sup>-1</sup>) together with high CH<sub>4</sub> regenerabilities (78.5, 80.4, and 78.5%).

Table 2 lists the membrane-based separation performances of top 20 MOF adsorbents for CH<sub>4</sub>/N<sub>2</sub> separation where they show similar performances in terms of membrane selectivity and CH<sub>4</sub> permeability. Considering CH<sub>4</sub>/N<sub>2</sub> membrane selectivity and CH<sub>4</sub> permeability in equal weight, cuf\_818 (F–OCH<sub>3</sub> functionalized), cuf\_2872 (F–NH<sub>2</sub> functionalized), and cuf\_1627 (F–OCH<sub>3</sub> functionalized) were identified as the top three membranes for the CH<sub>4</sub>/N<sub>2</sub> membrane-based separation with CH<sub>4</sub>/N<sub>2</sub> membrane selectivities and CH<sub>4</sub> permeabilities of 5.3, 4.5, and 5.0 and 5.74 × 10<sup>5</sup>, 5.47 × 10<sup>5</sup>, and 4.51 × 10<sup>5</sup> Barrer, respectively. An apparent geometric commonality of them is their narrow PLDs (around 4–6 Å) and mediocre void fractions (around 0.55–0.60). As the diffusion selectivities of top 20 MOF adsorbents are near 1 (sorbates diffuse at similar rates), the membrane selectivities are governed by the adsorption selectivities. Similarly, the higher CH<sub>4</sub> permeabilities (compared to N<sub>2</sub> permeabilities) are mostly due to higher amounts of CH<sub>4</sub> captured in the membranes.

### 3.4 N<sub>2</sub>/H<sub>2</sub> separation

Fig. S4† illustrates the N<sub>2</sub>/H<sub>2</sub> separation performance metrics of the MOFs in tandem with their textural features. The top panels demonstrate that, in general, the more N<sub>2</sub> selective MOFs have higher N<sub>2</sub> working capacities and smaller void fractions. The ranges of N<sub>2</sub>/H<sub>2</sub> selectivity, N<sub>2</sub> working

**Table 2** 20 best MOF adsorbents identified for the CH<sub>4</sub>/N<sub>2</sub> separation in tandem with their membrane-based separation performances

| Structure | $S_{\text{ads,CH}_4/\text{N}_2}$ | $\Delta N_{\text{CH}_4}$<br>(mol kg <sup>-1</sup> ) | $R_{\text{CH}_4}$ (%) | $S_{\text{diff,CH}_4/\text{N}_2}$ | $S_{\text{mem,CH}_4/\text{N}_2}$ | $D_{\text{self,CH}_4}$ (m <sup>2</sup> s <sup>-1</sup> ) | $D_{\text{self,N}_2}$ (m <sup>2</sup> s <sup>-1</sup> ) | $P_{\text{CH}_4}$ (Barrer) | $P_{\text{N}_2}$ (Barrer) |
|-----------|----------------------------------|---|-----------------------|-----------------------------------|----------------------------------|--|---|----------------------------|---------------------------|
| cuf_2878  | 4.6                              | 4.5   | 78.5                  | 1.04                              | 4.8                              | 1.51 × 10 <sup>-8</sup>                                  | 1.46 × 10 <sup>-8</sup>                                 | 4.59 × 10 <sup>5</sup>     | 9.39 × 10 <sup>4</sup>    |
| cuf_1627  | 4.7                              | 4.2   | 80.4                  | 1.05                              | 5.0                              | 1.59 × 10 <sup>-8</sup>                                  | 1.51 × 10 <sup>-8</sup>                                 | 4.51 × 10 <sup>5</sup>     | 8.88 × 10 <sup>4</sup>    |
| cuf_586   | 4.5                              | 4.4   | 78.5                  | 0.97                              | 4.4                              | 1.08 × 10 <sup>-8</sup>                                  | 1.11 × 10 <sup>-8</sup>                                 | 3.20 × 10 <sup>5</sup>     | 7.15 × 10 <sup>4</sup>    |
| cuf_810   | 4.7                              | 4.1   | 79.4                  | 0.83                              | 3.9                              | 7.15 × 10 <sup>-9</sup>                                  | 8.59 × 10 <sup>-9</sup>                                 | 2.05 × 10 <sup>5</sup>     | 5.15 × 10 <sup>4</sup>    |
| cuf_1633  | 4.8                              | 4.0   | 78.6                  | 1.04                              | 5.0                              | 1.14 × 10 <sup>-8</sup>                                  | 1.10 × 10 <sup>-8</sup>                                 | 3.19 × 10 <sup>5</sup>     | 6.26 × 10 <sup>4</sup>    |
| cuf_811   | 4.6                              | 4.1   | 80.8                  | 0.85                              | 3.9                              | 1.01 × 10 <sup>-8</sup>                                  | 1.18 × 10 <sup>-8</sup>                                 | 2.84 × 10 <sup>5</sup>     | 7.13 × 10 <sup>4</sup>    |
| cuf_735   | 4.1                              | 4.6   | 80.5                  | 1.09                              | 4.5                              | 1.77 × 10 <sup>-8</sup>                                  | 1.61 × 10 <sup>-8</sup>                                 | 4.57 × 10 <sup>5</sup>     | 1.01 × 10 <sup>5</sup>    |
| cuf_818   | 4.9                              | 4.0   | 75.8                  | 1.08                              | 5.3                              | 1.87 × 10 <sup>-8</sup>                                  | 1.73 × 10 <sup>-8</sup>                                 | 5.74 × 10 <sup>5</sup>     | 1.06 × 10 <sup>5</sup>    |
| pMOF_44   | 4.0                              | 4.4   | 82.6                  | 0.87                              | 3.5                              | 1.25 × 10 <sup>-8</sup>                                  | 1.43 × 10 <sup>-8</sup>                                 | 3.36 × 10 <sup>5</sup>     | 9.42 × 10 <sup>4</sup>    |
| cuf_2872  | 4.4                              | 4.2   | 79.9                  | 1.02                              | 4.5                              | 1.91 × 10 <sup>-8</sup>                                  | 1.87 × 10 <sup>-8</sup>                                 | 5.47 × 10 <sup>5</sup>     | 1.20 × 10 <sup>5</sup>    |
| cuf_7134  | 5.0                              | 3.8   | 77.2                  | 1.05                              | 5.2                              | 1.17 × 10 <sup>-8</sup>                                  | 1.12 × 10 <sup>-8</sup>                                 | 3.37 × 10 <sup>5</sup>     | 6.34 × 10 <sup>4</sup>    |
| cuf_809   | 4.4                              | 4.2   | 79.7                  | 0.95                              | 4.1                              | 1.68 × 10 <sup>-8</sup>                                  | 1.78 × 10 <sup>-8</sup>                                 | 4.46 × 10 <sup>5</sup>     | 1.06 × 10 <sup>5</sup>    |
| pMOF_513  | 3.5                              | 4.8   | 84.2                  | 0.96                              | 3.4                              | 1.91 × 10 <sup>-8</sup>                                  | 2.00 × 10 <sup>-8</sup>                                 | 4.56 × 10 <sup>5</sup>     | 1.34 × 10 <sup>5</sup>    |
| cuf_824   | 5.0                              | 3.9   | 73.9                  | 0.91                              | 4.5                              | 1.22 × 10 <sup>-8</sup>                                  | 1.34 × 10 <sup>-8</sup>                                 | 3.75 × 10 <sup>5</sup>     | 8.10 × 10 <sup>4</sup>    |
| cuf_110   | 4.9                              | 4.1   | 73.0                  | 0.80                              | 3.9                              | 5.03 × 10 <sup>-9</sup>                                  | 6.32 × 10 <sup>-9</sup>                                 | 1.51 × 10 <sup>5</sup>     | 3.84 × 10 <sup>4</sup>    |
| cuf_2640  | 4.2                              | 4.4   | 79.5                  | 1.06                              | 4.4                              | 1.49 × 10 <sup>-8</sup>                                  | 1.41 × 10 <sup>-8</sup>                                 | 4.10 × 10 <sup>5</sup>     | 9.08 × 10 <sup>4</sup>    |
| cuf_7812  | 4.2                              | 4.3   | 81.5                  | 1.11                              | 4.6                              | 1.00 × 10 <sup>-8</sup>                                  | 9.00 × 10 <sup>-9</sup>                                 | 2.61 × 10 <sup>5</sup>     | 5.54 × 10 <sup>4</sup>    |
| pMOF_41   | 3.8                              | 4.5   | 84.6                  | 0.99                              | 3.7                              | 1.40 × 10 <sup>-8</sup>                                  | 1.41 × 10 <sup>-8</sup>                                 | 3.46 × 10 <sup>5</sup>     | 9.10 × 10 <sup>4</sup>    |
| cuf_533   | 4.5                              | 4.1   | 78.9                  | 0.93                              | 4.1                              | 1.70 × 10 <sup>-8</sup>                                  | 1.84 × 10 <sup>-8</sup>                                 | 4.78 × 10 <sup>5</sup>     | 1.14 × 10 <sup>5</sup>    |
| cuf_340   | 4.2                              | 4.3   | 79.7                  | 0.86                              | 3.6                              | 1.13 × 10 <sup>-8</sup>                                  | 1.32 × 10 <sup>-8</sup>                                 | 3.11 × 10 <sup>5</sup>     | 8.50 × 10 <sup>4</sup>    |



capacity, and  $N_2$  regenerability are 2.0–11.7, 0.1–0.5 mol  $kg^{-1}$ , and 88.6–90.9%, respectively. Among them, *cuf\_916* and *cuf\_110* stand out from the rest with high  $N_2/H_2$  selectivities (11.7 and 11.0) and large  $N_2$  working capacities ( $\sim 0.4$  and  $\sim 0.5$  mol  $kg^{-1}$ ). The bottom panels reveal that those highly  $N_2$  selective (and regenerable) MOFs can have significant confinement effects as they possess relatively small PLDs and surface areas. Benchmarking  $N_2/H_2$  separation potentials of MOFs with others above, it can be concluded that the performance–performance or performance–property trends are similar in all gas separations despite having somewhat different ranges. This can be ascribed to different interaction strengths of adsorbates (*i.e.*, varying levels of adsorbate competition due to different LJ parameters, and presence/absence of

quadrupole moment) and slightly different lists of MOFs investigated for each separation as a result of structural filtering.

Fig. 6 depicts the  $N_2/H_2$  separation performance metrics of the MOFs categorized by functional groups. The top left panel shows that bare MOFs are one of the least  $N_2$  selective MOFs while MOFs functionalized with  $-OCH_3-OCH_3$  are the most  $N_2$  selective MOFs on average. However, it is noteworthy that some of the  $-NH_2$  functionalized MOFs (functionalized with  $-NH_2-NH_2$  and  $-F-NH_2$ ) attain the highest  $N_2/H_2$  selectivities. The top right panel demonstrates that MOFs functionalized with  $-NH_2-OCH_3$  have one of the largest spreads in  $N_2$  working capacities, and the highest mean  $N_2$  working capacities. Considering the extend of  $N_2$  working capacities attained by bare MOFs, this suggests that

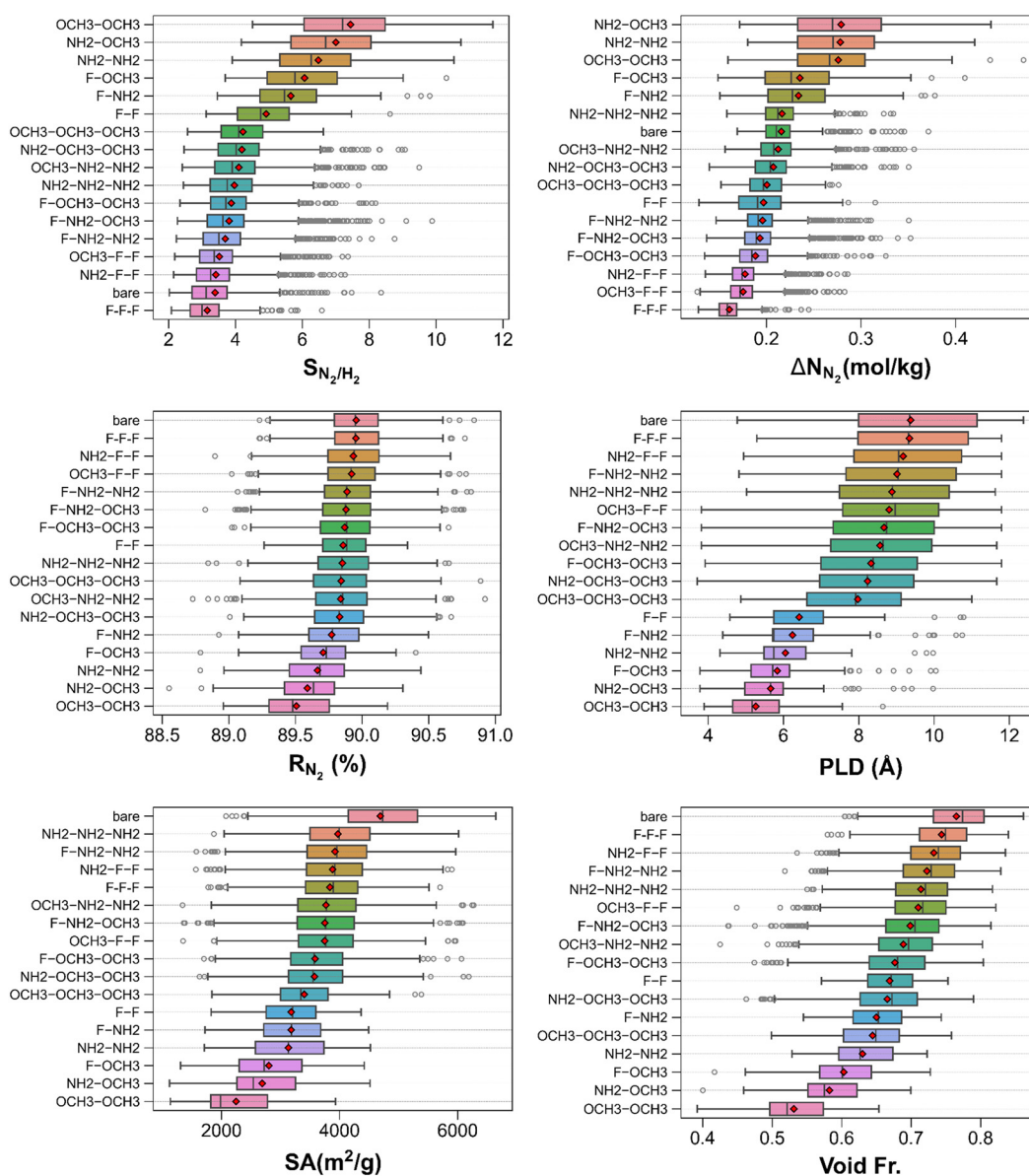


Fig. 6 Classification of  $N_2/H_2$  separation performance metrics and structural features of MOFs by functional groups.



functionalizing two linkers of bare MOFs can increase the N<sub>2</sub> working capacities considerably. In contrast, MOFs functionalized with -F-F-F show very narrow N<sub>2</sub> working capacity range and the smallest mean N<sub>2</sub> working capacity value hinting that functionalizing all linkers with -F groups is unfavorable for N<sub>2</sub> separation from H<sub>2</sub>. It can be deduced from the middle-left panel that all MOF groups attain very similar N<sub>2</sub> regenerabilities on average as well as close minimum/maximum values suggesting that the effect of functionalization on N<sub>2</sub> regenerability is not significant as opposed to that on N<sub>2</sub>/H<sub>2</sub> selectivity or N<sub>2</sub> working capacity. The other panels suggest that the textural properties of MOFs used for the N<sub>2</sub>/H<sub>2</sub> separation are very similar to those of MOFs probed for the separation of other three gas mixtures.

Table S6† shows the top 20 MOFs for the N<sub>2</sub>/H<sub>2</sub> separation whose N<sub>2</sub>/H<sub>2</sub> selectivity, N<sub>2</sub> working capacity, and N<sub>2</sub> regenerability span the ranges of 8.9–11.7, 0.4–0.5 mol kg<sup>-1</sup>, and 88.6–90.0%, respectively. These MOFs have a wide variety of textural properties as evidenced by their PLDs of 3.94–5.74 Å, surface areas of 1136.1–2445.9 m<sup>2</sup> g<sup>-1</sup>, void fractions of 0.437–0.585, and pore volumes of 0.455–0.711 cm<sup>3</sup> g<sup>-1</sup>. The best three MOFs are *cuf\_110*, *cuf\_916*, and *cuf\_824* which are -NH<sub>2</sub> and -OCH<sub>3</sub> functionalized MOFs (specifically, -OCH<sub>3</sub>-OCH<sub>3</sub>, -OCH<sub>3</sub>-OCH<sub>3</sub>, and -NH<sub>2</sub>-OCH<sub>3</sub>, respectively) attaining N<sub>2</sub>/H<sub>2</sub> selectivities of 11.0, 11.7, and 10.7, N<sub>2</sub> working capacities of 0.5, 0.4, and 0.4, and N<sub>2</sub> regenerabilities of 89.0, 89.5, and 89.3%, successively (linker representations for all the top MOFs can be found in Tables S7–S10†).

Having identified the best structures for adsorption and membrane-based separations, we now turn to the performance benchmarks for various types of materials. As for CF<sub>4</sub>/CH<sub>4</sub> separation, the top three adsorbents (*pMOF\_10*, *pMOF\_26*, and *pMOF\_8*) identified in this work exhibit higher CF<sub>4</sub>/CH<sub>4</sub> selectivities and CF<sub>4</sub> working capacities than those of top Zr-MOFs reported earlier (up to 5.1 and 2.1 mol kg<sup>-1</sup>, respectively, at the same conditions as in this work).<sup>15</sup> While the regenerabilities of these MTV-MOFs are less than those of top two Zr-MOFs (72–81% vs. ~84–85%), in practical terms, this may not lead to a significant discrepancy in separation performances as the differences in regenerabilities across top MTV-MOFs and Zr-MOFs are minor. To the best of our knowledge, the top performances (CF<sub>4</sub>/CH<sub>4</sub> selectivity ≥ 6.0 and CF<sub>4</sub> working capacity ≥ 2.7 mol kg<sup>-1</sup>) observed in this work imply the highest values reported so far suggesting the potential use of bare MOFs for the CF<sub>4</sub>/CH<sub>4</sub> separation. The higher selectivities of top MTV-MOFs with respect to top Zr-MOFs can be attributed to narrower pore sizes of MTV-MOFs providing tighter CF<sub>4</sub> fits. It has been observed that the narrower pores also lead to two-three folds higher adsorption amounts in top MTV-MOFs compared to top Zr-MOFs at the desorption pressure (0.1 bar). At the first glance, this might lead to an impression that MTV-MOFs could not achieve high CF<sub>4</sub> working capacities. However, stronger confinement effects together with larger adsorbate–adsorbate interactions in MTV-MOFs lead to significantly different adsorption

amounts (~3.4–4.0 mol kg<sup>-1</sup> for MTV-MOFs vs. ~2.3–2.8 mol kg<sup>-1</sup>) at the adsorption pressure (1 bar) leading to ~30–40% higher working capacities.

Comparing the hypothetical MOFs' CH<sub>4</sub>/H<sub>2</sub> separation, it can be inferred that similar adsorption and membrane-based separation performances may be obtained by other MOFs. For instance, in a computational study,<sup>24</sup> the top performing MOF adsorbents (based on adsorbent performance score) were determined to possess CH<sub>4</sub>/H<sub>2</sub> adsorption selectivities of ~25–30 and CH<sub>4</sub> working capacities of ~4–6 mol kg<sup>-1</sup>. In another computational work,<sup>23</sup> an initial MOF membrane screening based on Henry's constants and self-diffusivities calculated at infinite dilution conditions revealed that CH<sub>4</sub>/H<sub>2</sub> membrane selectivities similar to/higher than those reported in this work could be attained. While a large portion of the MOFs have CH<sub>4</sub>/H<sub>2</sub> membrane selectivities between 1 and 10, the highest CH<sub>4</sub>/H<sub>2</sub> adsorption selectivities were above 1000. However, as the effects of presence of multiple sorbate types in materials and higher adsorption pressure were not considered in those calculations, those selectivities could change drastically at the conditions specified in this work.

A recent large-scale screening study<sup>31</sup> on MOFs showed that many MOFs screened in that work have similar or worse CH<sub>4</sub>/N<sub>2</sub> adsorption-based separation performances (CH<sub>4</sub>/N<sub>2</sub> adsorption selectivities between 0.6 and 5, CH<sub>4</sub> working capacities up to 4 mol kg<sup>-1</sup>) than those in the top 20 list of this work. However, they have also identified a few MOFs that can potentially perform better than the hypothetical MOFs studied in this work as they could have CH<sub>4</sub>/N<sub>2</sub> adsorption selectivity larger than 8 or CH<sub>4</sub> working capacity bigger than 5 mol kg<sup>-1</sup>. It is worthwhile to note that those cases also involve trade-offs across at least two metrics (*e.g.*, adsorption selectivity vs. working capacity) and their overall performances may still be comparable to the top adsorbents determined in this work. Yan *et al.*<sup>30</sup> performed high-throughput screening of computation-ready, experimental (CoRE) MOFs<sup>58</sup> for the CH<sub>4</sub>/N<sub>2</sub> separation around ambient conditions and determined that some of the MOFs can achieve CH<sub>4</sub>/N<sub>2</sub> selectivities ~20. While such selectivities seem much higher than those of top MTV-MOFs identified in this work, it should be reminded that they were attained at a lower adsorption pressure than that in this work (1 vs. 10 bar). While one can typically expect selectivity to drop at higher pressure due to weaker host–guest interactions, it is also possible to observe a cooperative effect between sorbates enhancing the selectivity.<sup>59</sup> Thus, such comparisons should preferably be made after obtaining selectivities at the same pressure conditions.

As to the N<sub>2</sub>/H<sub>2</sub> separation, the range of N<sub>2</sub>/H<sub>2</sub> adsorption selectivity values (~9–11) might look considerably smaller than those (N<sub>2</sub>/H<sub>2</sub> adsorption selectivity up to ~100) reported by Azar *et al.*<sup>34</sup> However, in the latter work, the competition effects between the sorbates are not considered (infinite dilution conditions) which hinders a one-to-one comparison. While the N<sub>2</sub>/H<sub>2</sub> adsorption selectivities of the hypothetical



MOFs investigated in this work are relatively high, the limited N<sub>2</sub> working capacities of the hypothetical MOFs may bring about economic challenges for the selective N<sub>2</sub> removal from H<sub>2</sub>.

Before concluding, we would like to note a few aspects of our screening study. Firstly, the MTV-MOF structures obtained from the database<sup>38</sup> were used as they are (*i.e.*, unoptimized structures). It has been shown earlier that structure optimizations (and optimization settings) may lead to considerably different gas uptakes.<sup>60</sup> For instance, it has been shown earlier that while Xe uptake at 298 K, 1 bar in experimentally determined structure of Ni(PyC)<sub>2</sub> matches that in one of its optimized counterparts (optimized with unit cell parameter constraints), it is overestimated by other optimized counterpart structures (optimized with unit cell angle constraints and no constraints).<sup>60</sup> Secondly, while the studied gas mixtures are assumed to be dry, in practice, they may include varying levels of humidity which can affect the separation performances (adsorption selectivity, membrane selectivity, gas permeability) of adsorbents and/or membranes.<sup>61</sup> As an example, Daglar *et al.*<sup>61</sup> demonstrated that the inclusion of H<sub>2</sub>O in CO<sub>2</sub>/N<sub>2</sub> mixture can hamper the adsorption and membrane selectivity together with gas permeabilities. However, as the simulations involving H<sub>2</sub>O are typically computationally very expensive, we have not carried out simulations to study separation of humid mixtures. Thirdly, while not considered in this study, the inclusion of framework flexibility in the simulations can be important for adsorption and/or membrane-based separations depending on the case.<sup>62–64</sup> Despite this fact, flexible frameworks were not employed in the simulations as universal and accurate flexible force-field parameters are not available in the literature for a diverse set of materials. Also, as the simulations employing flexible materials typically take much longer time than those with rigid materials, it would not be feasible to carry out simulations for the entire set of materials. It should be noted that the incorporation of flexibility effects does not invariably improve or worsen gas uptakes/selectivities of materials as the separation performances of materials are governed by an interplay of pore size, pore chemistry, and intrinsic flexibility.<sup>65</sup> Thus, the separation performances of top materials identified may enhance or deteriorate at varying levels depending on their pore sizes, chemistry and the extent of their flexibilities. To sum up, our computational exploration of MTV-MOFs has unraveled potentially useful adsorbents and membranes which can serve as the starting point for subsequent experimental and theoretical efforts.

## 4. Conclusions

In this work, the CF<sub>4</sub>/CH<sub>4</sub>, CH<sub>4</sub>/H<sub>2</sub>, CH<sub>4</sub>/N<sub>2</sub>, and N<sub>2</sub>/H<sub>2</sub> separation capabilities of MTV-MOFs were investigated. After filtering the structures based on geometric properties, the resulting list of materials have been studied using GCMC simulations to compute the uptakes of four different gas

mixtures under relevant separation conditions. The top adsorbents identified for each gas separation were found to have distinct properties such as different functional groups, and different ranges of pore size, pore volume *etc.* hinting at the disparate structural needs for different gas separation applications. While many different MTV-MOFs were tested for the adsorption-based separation of CF<sub>4</sub>/CH<sub>4</sub> mixture, interestingly, the top three MOFs were found to be bare MOFs. For the adsorption-based separation of CH<sub>4</sub>/H<sub>2</sub> and CH<sub>4</sub>/N<sub>2</sub> mixtures, MTV-MOFs with specific combinations of –NH<sub>2</sub>, –F, and –OCH<sub>3</sub> functional groups (*i.e.*, –NH<sub>2</sub>–NH<sub>2</sub>, –NH<sub>2</sub>–OCH<sub>3</sub>, and –F–OCH<sub>3</sub>) were determined to have the highest three rankings. Similarly, MTV-MOFs with –OCH<sub>3</sub>–OCH<sub>3</sub>, and –NH<sub>2</sub>–OCH<sub>3</sub> functional groups ranked as the top three for N<sub>2</sub>/H<sub>2</sub> separation. Comparison of adsorption-based separation performances of the MTV-MOFs that we considered in this work with the previously studied MOFs showed that MTV MOFs can outperform the latter in terms of one or more adsorption-based separation performance metrics. Our analysis on top three MOFs indicates that MOFs based on chrysene, pyrene, 2,6-naphthyridine, acetylenedicarboxylic acid (chrysene, 2,6-naphthyridine, and acetylenedicarboxylic acid) can be beneficial for CF<sub>4</sub>/CH<sub>4</sub>, CH<sub>4</sub>/N<sub>2</sub>, and N<sub>2</sub>/H<sub>2</sub> (CH<sub>4</sub>/H<sub>2</sub>) separation. For the CF<sub>4</sub>/CH<sub>4</sub> separation, it has been observed that many top materials involve pyrazine-based linkers as well. Having determined the top adsorbents, membrane-based separation performances of the top 20 materials for CH<sub>4</sub>/H<sub>2</sub> and CH<sub>4</sub>/N<sub>2</sub> separations were investigated combining the GCMC and MD results through which it has been deduced that the highest membrane selectivities were attained by MOFs with PLDs of ~5–6 Å and void fractions of ~0.55–0.60. For membrane-based separation of CH<sub>4</sub>/H<sub>2</sub> and CH<sub>4</sub>/N<sub>2</sub> mixtures, MTV-MOFs with –F, –NH<sub>2</sub>, and –F–OCH<sub>3</sub> functional groups demonstrated the best performances in terms of equally weighted membrane selectivity and CH<sub>4</sub> permeability. Overall, our results demonstrated that MTV-MOFs are quite promising for the CF<sub>4</sub>/CH<sub>4</sub> adsorption-based separation with the highest CF<sub>4</sub>/CH<sub>4</sub> selectivities and CF<sub>4</sub> working capacities reported so far. As for the CH<sub>4</sub>/H<sub>2</sub> and CH<sub>4</sub>/N<sub>2</sub> separation, MTV-MOFs show similar adsorption and/or membrane-based separation performances with respect to other MOFs investigated. While N<sub>2</sub>/H<sub>2</sub> adsorption selectivities of MTV-MOFs studied in this work appear lower than some of those in Azar *et al.*'s work,<sup>34</sup> the former is more relevant and accurate as it involves gas competition effects.

## Conflicts of interest

The authors declare no competing financial interest.

## Acknowledgements

S. K. acknowledges ERC-2017-Starting Grant. This study has received funding from the European Research Council (ERC) under the European Union's Horizon 2020 research and innovation programme (ERC-2017-Starting Grant, grant





agreement no. 756489-COSMOS). The numerical calculations reported in this paper were partially performed at TUBITAK ULAKBIM, High Performance and Grid Computing Center (TRUBA resources). Computing resources used in this work were partially provided by the National Center for High Performance Computing of Turkey (UHem) under grant number 1009312021.

## References

- C. A. Trickett, A. Helal, B. A. Al-Maythaly, Z. H. Yamani, K. E. Cordova and O. M. Yaghi, The Chemistry of Metal–Organic Frameworks for CO<sub>2</sub> Capture, Regeneration and Conversion, *Nat. Rev. Mater.*, 2017, **2**, 17045.
- X. Zhao, Y. Wang, D.-S. Li, X. Bu and P. Feng, Metal–Organic Frameworks for Separation, *Adv. Mater.*, 2018, **30**, 1705189.
- L. Jiao, Y. Wang, H.-L. Jiang and Q. Xu, Metal–Organic Frameworks as Platforms for Catalytic Applications, *Adv. Mater.*, 2018, **30**, 1703663.
- I. Stassen, N. Burtch, A. Talin, P. Falcaro, M. Allendorf and R. Ameloot, An Updated Roadmap for the Integration of Metal–Organic Frameworks with Electronic Devices and Chemical Sensors, *Chem. Soc. Rev.*, 2017, **46**, 3185–3241.
- J. Yang and Y.-W. Yang, Metal–Organic Frameworks for Biomedical Applications, *Small*, 2020, **16**, 1906846.
- J. Li, X. Wang, G. Zhao, C. Chen, Z. Chai, A. Alsaedi, T. Hayat and X. Wang, Metal–Organic Framework-Based Materials: Superior Adsorbents for the Capture of Toxic and Radioactive Metal Ions, *Chem. Soc. Rev.*, 2018, **47**, 2322–2356.
- K. Adil, Y. Belmabkhout, R. S. Pillai, A. Cadiau, P. M. Bhatt, A. H. Assen, G. Maurin and M. Eddaoudi, Gas/Vapour Separation Using Ultra-Microporous Metal–Organic Frameworks: Insights into the Structure/Separation Relationship, *Chem. Soc. Rev.*, 2017, **46**, 3402–3430.
- P. Z. Moghadam, A. Li, S. B. Wiggin, A. Tao, A. G. P. Maloney, P. A. Wood, S. C. Ward and D. Fairen-Jimenez, Development of a Cambridge Structural Database Subset: A Collection of Metal–Organic Frameworks for Past, Present, and Future, *Chem. Mater.*, 2017, **29**, 2618–2625.
- P. G. Boyd, A. Chidambaram, E. García-Díez, C. P. Ireland, T. D. Daff, R. Bounds, A. Gładysiak, P. Schouwink, S. M. Moosavi and M. M. Maroto-Valer, *et al.*, Data-Driven Design of Metal–Organic Frameworks for Wet Flue Gas CO<sub>2</sub> Capture, *Nature*, 2019, **576**, 253–256.
- Y. G. Chung, E. Haldoupis, B. J. Bucior, M. Haranczyk, S. Lee, H. Zhang, K. D. Vogiatzis, M. Milisavljevic, S. Ling and J. S. Camp, *et al.*, Advances, Updates, and Analytics for the Computation-Ready, Experimental Metal–Organic Framework Database: CoRE MOF 2019, *J. Chem. Eng. Data*, 2019, **64**, 5985–5998.
- S. W. Choi, D.-H. Lee, J. Kim, J. Kim, J.-H. Park, H. T. Beum, D.-S. Lim and K. B. Lee, A Titanium Carbide-Derived Novel Tetrafluoromethane Adsorbent with Outstanding Adsorption Performance, *Chem. Eng. J.*, 2017, **311**, 227–235.
- I. Senkovska, E. Barea, J. A. R. Navarro and S. Kaskel, Adsorptive Capturing and Storing Greenhouse Gases Such as Sulfur Hexafluoride and Carbon Tetrafluoride Using Metal–Organic Frameworks, *Microporous Mesoporous Mater.*, 2012, **156**, 115–120.
- Y. Guo, J. Hu, X. Liu, T. Sun, S. Zhao and S. Wang, Scalable Solvent-Free Preparation of [Ni<sub>3</sub>(HCOO)<sub>6</sub>] Frameworks for Highly Efficient Separation of CH<sub>4</sub> from N<sub>2</sub>, *Chem. Eng. J.*, 2017, **327**, 564–572.
- S. Calero, J. J. Gutiérrez-Sevillano and E. García-Pérez, Effect of the Molecular Interactions on the Separation of Nonpolar Mixtures Using Cu-BTC Metal–Organic Framework, *Microporous Mesoporous Mater.*, 2013, **165**, 79–83.
- H. Demir and S. Keskin, Zr-MOFs for CF<sub>4</sub>/CH<sub>4</sub>, CH<sub>4</sub>/H<sub>2</sub>, and CH<sub>4</sub>/N<sub>2</sub> Separation: Towards the Goal of Discovering Stable and Effective Adsorbents, *Mol. Syst. Des. Eng.*, 2021, **6**, 627–642.
- M. A. Moreira, R. O. M. Dias, U.-H. Lee, J.-S. Chang, A. M. Ribeiro, A. F. P. Ferreira and A. E. Rodrigues, Adsorption Equilibrium of Carbon Dioxide, Methane, Nitrogen, Carbon Monoxide, and Hydrogen on UiO-66(Zr)-(COOH)<sub>2</sub>, *J. Chem. Eng. Data*, 2019, **64**, 4724–4732.
- Z. Chen, P. Li, R. Anderson, X. Wang, X. Zhang, L. Robison, L. R. Redfern, S. Moribe, T. Islamoglu and D. A. Gómez-Gualdrón, *et al.*, Balancing Volumetric and Gravimetric Uptake in Highly Porous Materials for Clean Energy, *Science*, 2020, **368**, 297–303.
- M. D. Allendorf, Z. Hulvey, T. Gennett, A. Ahmed, T. Autrey, J. Camp, E. Seon Cho, H. Furukawa, M. Haranczyk and M. Head-Gordon, *et al.*, An Assessment of Strategies for the Development of Solid-State Adsorbents for Vehicular Hydrogen Storage, *Energy Environ. Sci.*, 2018, **11**, 2784–2812.
- B. Liu, Q. Yang, C. Xue, C. Zhong, B. Chen and B. Smit, Enhanced Adsorption Selectivity of Hydrogen/Methane Mixtures in Metal–Organic Frameworks with Interpenetration: A Molecular Simulation Study, *J. Phys. Chem. C*, 2008, **112**, 9854–9860.
- M. Gallo and D. Glossman-Mitnik, Fuel Gas Storage and Separations by Metal–Organic Frameworks: Simulated Adsorption Isotherms for H<sub>2</sub> and CH<sub>4</sub> and Their Equimolar Mixture, *J. Phys. Chem. C*, 2009, **113**, 6634–6642.
- S. Qiu, M. Xue and G. Zhu, Metal–Organic Framework Membranes: From Synthesis to Separation Application, *Chem. Soc. Rev.*, 2014, **43**, 6116–6140.
- H. Daglar and S. Keskin, Recent Advances, Opportunities, and Challenges in High-Throughput Computational Screening of MOFs for Gas Separations, *Coord. Chem. Rev.*, 2020, **422**, 213470.
- C. Altintas, G. Avci, H. Daglar, E. Gulcay, I. Erucar and S. Keskin, Computer Simulations of 4240 MOF Membranes for H<sub>2</sub>/CH<sub>4</sub> Separations: Insights into Structure–Performance Relations, *J. Mater. Chem. A*, 2018, **6**, 5836–5847.
- C. Altintas, I. Erucar and S. Keskin, High-Throughput Computational Screening of the Metal Organic Framework Database for CH<sub>4</sub>/H<sub>2</sub> Separations, *ACS Appl. Mater. Interfaces*, 2018, **10**, 3668–3679.
- T.-H. Kim, S.-Y. Kim, T.-U. Yoon, M.-B. Kim, W. Park, H. H. Han, C. Kong, C.-Y. Park, J.-H. Kim and Y.-S. Bae, Improved



- Methane/Nitrogen Separation Properties of Zirconium-Based Metal–Organic Framework by Incorporating Highly Polarizable Bromine Atoms, *Chem. Eng. J.*, 2020, **399**, 125717.
- 26 X. Wu, B. Yuan, Z. Bao and S. Deng, Adsorption of Carbon Dioxide, Methane and Nitrogen on an Ultramicroporous Copper Metal–Organic Framework, *J. Colloid Interface Sci.*, 2014, **430**, 78–84.
- 27 J. Hu, T. Sun, X. Liu, Y. Guo and S. Wang, Separation of CH<sub>4</sub>/N<sub>2</sub> Mixtures in Metal–Organic Frameworks with 1D Micro-Channels, *RSC Adv.*, 2016, **6**, 64039–64046.
- 28 J. Hu, T. Sun, X. Liu, S. Zhao and S. Wang, Rationally Tuning the Separation Performances of [M<sub>3</sub>(HCOO)<sub>6</sub>] Frameworks for CH<sub>4</sub>/N<sub>2</sub> Mixtures via Metal Substitution, *Microporous Mesoporous Mater.*, 2016, **225**, 456–464.
- 29 Z. Sumer and S. Keskin, Adsorption- and Membrane-Based CH<sub>4</sub>/N<sub>2</sub> Separation Performances of MOFs, *Ind. Eng. Chem. Res.*, 2017, **56**, 8713–8722.
- 30 T. Yan, Y. Lan, D. Liu, Q. Yang and C. Zhong, Large-Scale Screening and Design of Metal–Organic Frameworks for CH<sub>4</sub>/N<sub>2</sub> Separation, *Chem. - Asian J.*, 2019, **14**, 3688–3693.
- 31 H. C. Gulbalkan, Z. P. Haslak, C. Altintas, A. Uzun and S. Keskin, Assessing CH<sub>4</sub>/N<sub>2</sub> Separation Potential of MOFs, COFs, IL/MOF, MOF/Polymer, and COF/Polymer Composites, *Chem. Eng. J.*, 2021, 131239.
- 32 B. Mu, P. M. Schoenecker and K. S. Walton, Gas Adsorption Study on Mesoporous Metal–Organic Framework UCM-1, *J. Phys. Chem. C*, 2010, **114**, 6464–6471.
- 33 M. J. Regufe, J. Tamajon, A. M. Ribeiro, A. Ferreira, U.-H. Lee, Y. K. Hwang, J.-S. Chang, C. Serre, J. M. Loureiro and A. E. Rodrigues, Syngas Purification by Porous Amino-Functionalized Titanium Terephthalate MIL-125, *Energy Fuels*, 2015, **29**, 4654–4664.
- 34 A. N. V. Azar, S. Velioglu and S. Keskin, Large-Scale Computational Screening of Metal Organic Framework (MOF) Membranes and MOF-Based Polymer Membranes for H<sub>2</sub>/N<sub>2</sub> Separations, *ACS Sustainable Chem. Eng.*, 2019, **7**, 9525–9536.
- 35 A. Kirchon, L. Feng, H. F. Drake, E. A. Joseph and H.-C. Zhou, From Fundamentals to Applications: A Toolbox for Robust and Multifunctional MOF Materials, *Chem. Soc. Rev.*, 2018, **47**, 8611–8638.
- 36 Y.-B. Zhang, H. Furukawa, N. Ko, W. Nie, H. J. Park, S. Okajima, K. E. Cordova, H. Deng, J. Kim and O. M. Yaghi, Introduction of Functionality, Selection of Topology, and Enhancement of Gas Adsorption in Multivariate Metal–Organic Framework-177, *J. Am. Chem. Soc.*, 2015, **137**, 2641–2650.
- 37 Z. Hu, A. Gami, Y. Wang and D. Zhao, A Triphasic Modulated Hydrothermal Approach for the Synthesis of Multivariate Metal–Organic Frameworks with Hydrophobic Moieties for Highly Efficient Moisture-Resistant CO<sub>2</sub> Capture, *Adv. Sustainable Syst.*, 2017, **1**, 1700092.
- 38 S. Li, Y. G. Chung, C. M. Simon and R. Q. Snurr, High-Throughput Computational Screening of Multivariate Metal–Organic Frameworks (MTV-MOFs) for CO<sub>2</sub> Capture, *J. Phys. Chem. Lett.*, 2017, **8**, 6135–6141.
- 39 T. F. Willems, C. H. Rycroft, M. Kazi, J. C. Meza and M. Haranczyk, Algorithms and Tools for High-Throughput Geometry-Based Analysis of Crystalline Porous Materials, *Microporous Mesoporous Mater.*, 2012, **149**, 134–141.
- 40 D. Ongari, P. G. Boyd, S. Barthel, M. Witman, M. Haranczyk and B. Smit, Accurate Characterization of the Pore Volume in Microporous Crystalline Materials, *Langmuir*, 2017, **33**, 14529–14538.
- 41 E. Haldoupis, S. Nair and D. S. Sholl, Efficient Calculation of Diffusion Limitations in Metal Organic Framework Materials: A Tool for Identifying Materials for Kinetic Separations, *J. Am. Chem. Soc.*, 2010, **132**, 7528–7539.
- 42 D. Dubbeldam, S. Calero, D. E. Ellis and R. Q. Snurr, RASPA: Molecular Simulation Software for Adsorption and Diffusion in Flexible Nanoporous Materials, *Mol. Simul.*, 2016, **42**, 81–101.
- 43 M. Heuchel, R. Q. Snurr and E. Buss, Adsorption of CH<sub>4</sub>–CF<sub>4</sub> Mixtures in Silicalite: Simulation, Experiment, and Theory, *Langmuir*, 1997, **13**, 6795–6804.
- 44 I. Erucar and S. Keskin, Computational Assessment of MOF Membranes for CH<sub>4</sub>/H<sub>2</sub> Separations, *J. Membr. Sci.*, 2016, **514**, 313–321.
- 45 D. Wu, C. Wang, B. Liu, D. Liu, Q. Yang and C. Zhong, Large-Scale Computational Screening of Metal-Organic Frameworks for CH<sub>4</sub>/H<sub>2</sub> Separation, *AIChE J.*, 2012, **58**, 2078–2084.
- 46 O. C. David, D. Gorri, K. Nijmeijer, I. Ortiz and A. Urriaga, Hydrogen Separation from Multicomponent Gas Mixtures Containing CO, N<sub>2</sub> and CO<sub>2</sub> Using Matrimid® Asymmetric Hollow Fiber Membranes, *J. Membr. Sci.*, 2012, **419–420**, 49–56.
- 47 M. A. Nadeem, A. W. Thornton, M. R. Hill and J. A. Stride, A Flexible Copper Based Microporous Metal–Organic Framework Displaying Selective Adsorption of Hydrogen over Nitrogen, *Dalton Trans.*, 2011, **40**, 3398–3401.
- 48 S.-H. Choi, A. Brunetti, E. Drioli and G. Barbieri, H<sub>2</sub> Separation From H<sub>2</sub>/N<sub>2</sub> and H<sub>2</sub>/CO Mixtures with Co-Polyimide Hollow Fiber Module, *Sep. Sci. Technol.*, 2010, **46**, 1–13.
- 49 A. K. Rappe, C. J. Casewit, K. S. Colwell, W. A. Goddard and W. M. Skiff, UFF, a Full Periodic Table Force Field for Molecular Mechanics and Molecular Dynamics Simulations, *J. Am. Chem. Soc.*, 1992, **114**, 10024–10035.
- 50 S. Kancharlapalli, A. Gopalan, M. Haranczyk and R. Q. Snurr, Fast and Accurate Machine Learning Strategy for Calculating Partial Atomic Charges in Metal–Organic Frameworks, *J. Chem. Theory Comput.*, 2021, **17**, 3052–3064.
- 51 A. I. Skoulidas, T. C. Bowen, C. M. Doelling, J. L. Falconer, R. D. Noble and D. S. Sholl, Comparing Atomistic Simulations and Experimental Measurements for CH<sub>4</sub>/CF<sub>4</sub> Mixture Permeation through Silicalite Membranes, *J. Membr. Sci.*, 2003, **227**, 123–136.
- 52 M. G. Martin and J. I. Siepmann, Transferable Potentials for Phase Equilibria. 1. United-Atom Description of n-Alkanes, *J. Phys. Chem. B*, 1998, **102**, 2569–2577.
- 53 J. J. Potoff and J. I. Siepmann, Vapor–Liquid Equilibria of Mixtures Containing Alkanes, Carbon Dioxide, and Nitrogen, *AIChE J.*, 2001, **47**, 1676–1682.



- 54 V. Buch, Path Integral Simulations of Mixed Para-D<sub>2</sub> and Ortho-D<sub>2</sub> Clusters: The Orientational Effects, *J. Chem. Phys.*, 1994, **100**, 7610–7629.
- 55 P. P. Ewald, The Calculation of Optical and Electrostatic Grid Potential, *Ann. Phys.*, 1921, **64**, 253–287.
- 56 D. Frenkel and B. Smit, *Understanding Molecular Simulation: From Algorithms to Applications*, Academic Press, San Diego, CA, 2002.
- 57 A. Einstein, *Investigations on the Theory of the Brownian Movement*, Courier Corporation, New York, 1956.
- 58 Y. G. Chung, J. Camp, M. Haranczyk, B. J. Sikora, W. Bury, V. Krungleviciute, T. Yildirim, O. K. Farha, D. S. Sholl and R. Q. Snurr, Computation-Ready, Experimental Metal–Organic Frameworks: A Tool To Enable High-Throughput Screening of Nanoporous Crystals, *Chem. Mater.*, 2014, **26**, 6185–6192.
- 59 E. Ren and F.-X. Coudert, Thermodynamic Exploration of Xenon/Krypton Separation Based on a High-Throughput Screening, *Faraday Discuss.*, 2021, **231**, 201–223.
- 60 N. Gantzer, M.-B. Kim, A. Robinson, M. W. Terban, S. Ghose, R. E. Dinnebier, A. H. York, D. Tiana, C. M. Simon and P. K. Thallapally, Computation-Informed Optimization of Ni(PyC)<sub>2</sub> Functionalization for Noble Gas Separations, *ChemRxiv*, 2021, preprint, DOI: [10.26434/chemrxiv-2021-sr171](https://doi.org/10.26434/chemrxiv-2021-sr171).
- 61 H. Daglar and S. Keskin, Computational Screening of Metal–Organic Frameworks for Membrane-Based CO<sub>2</sub>/N<sub>2</sub>/H<sub>2</sub>O Separations: Best Materials for Flue Gas Separation, *J. Phys. Chem. C*, 2018, **122**, 17347–17357.
- 62 Z. Yu, D. M. Anstine, S. E. Boulfefel, C. Gu, C. M. Colina and D. S. Sholl, Incorporating Flexibility Effects into Metal–Organic Framework Adsorption Simulations Using Different Models, *ACS Appl. Mater. Interfaces*, 2021, **13**, 61305–61315.
- 63 C. Altintas and S. Keskin, Molecular Simulations of MOF Membranes and Performance Predictions of MOF/Polymer Mixed Matrix Membranes for CO<sub>2</sub>/CH<sub>4</sub> Separations, *ACS Sustainable Chem. Eng.*, 2019, **7**, 2739–2750.
- 64 I. Erucar and S. Keskin, Computational Modeling of Bio-MOFs for CO<sub>2</sub>/CH<sub>4</sub> Separations, *Chem. Eng. Sci.*, 2015, **130**, 120–128.
- 65 M. Witman, S. Ling, S. Jawahery, P. G. Boyd, M. Haranczyk, B. Slater and B. Smit, The Influence of Intrinsic Framework Flexibility on Adsorption in Nanoporous Materials, *J. Am. Chem. Soc.*, 2017, **139**, 5547–5557.
- 66 O. F. Altundal, Z. P. Haslak and S. Keskin, *Ind. Eng. Chem. Res.*, 2021, **60**(35), 12999–13012.
- 67 Y. Lim and J. Kim, *Mol. Syst. Des. Eng.*, 2022, **7**, 1056–1064.

